Solvent-assisted Nanolithography on Polystyrene Surfaces by Nanoindentation with the Atomic Force Microscope

Master's Thesis

for attainment of the degree

Master of Science
(M.Sc. in Chemistry)

submitted by

Yuting Sun

Department 8 (Chemistry-Biology)
University of Siegen
2007

The Master's Thesis submitted was completed between 01.05.07 and 31.12.07 in the Max-Planck Institute for Polymer Research as the final requirement for the fourth-semester course of study in Chemistry (Degree: Master of Science) at the University of Siegen in the Department of Chemistry-Biology under the supervision of Prof. Dr. Hans-Jürgen Butt.

INDEX

1. Introduction

Nanolithography is a term used to describe a number of techniques for creating structures in the scale of nanometers. Generation of nanostructures can be categorized by two main methods: top-down and bottom-up. The top-down approach creates nanoscale patterns from a featureless starting material, while the bottom-up route creates two- and three-dimensional structures by using interactions of molecules and/or colloidal particles. [1] Photolithography [2, 3], electron beam lithography [4, 5] and focused ion beam lithography [6, 7] are examples of typical techniques of the top-down approach. They are widely used in semiconductor manufacturing, but limited by high operating cost and poor accessibility. Several novel low cost methods have also been developed for nanoscale pattern formation and replication. Atomic Force Microscope (AFM) based nanolithography is one of these methods.

AFM based nanolithography is a unique tool for modification and nano structuring of the substrate. AFM can be operated in liquid, air or vacuum, and it can be applied to every kind of sample, including metals [8] semiconductors [9] and resist layers on semiconductors [10], Langmuir-Blodgett films [11], and polymer films [12]. Since polymers are soft materials and widely used as masks or resists, there are strong interests in the patterning of polymers by AFM nanolithography. A novel method developed by Cappella and Bonaccurso, which is called solvent assisted nanolithography, can generate relief structures on polystyrene surfaces. [13] Cappella and Bonaccurso found that by exposing plasma-treated polystyrene plates indented by AFM-tips to solvent vapor, two-dimensional arrays of conical protuberances are formed on the surface of polymers.

In the method they presented, three steps were required:

1) The plasma treatment of the polymer to create a superficial cross-linked layer which protects the polymer surface from swelling.
2) Indentation by AFM tips to pierce the superficial cross-linked layer and produce via-holes.

3) Exposure to solvent for making the under layering non-cross-linked polymer to swell out of the holes.

The corresponding parameters which influence the cone growth process are:

1) Time and power of plasma treatment, which control the stiffness and the thickness of the superficial cross-linked layer.
2) Maximum force load of the indentation, which determines the depth and the width of the carved holes.
3) Concentration of the solvent and exposure time, which affect the growth speed and the final size.

They found the volume of the conical structures fits an exponential function of exposure time, and so do the diameters and heights of the cones. The aspect ratio was nearly constant. To apply this technique to lithography, it is necessary to control the growth and the dimensions of the nanostructures.

Solvent concentration and exposure time were not well controlled in that experiment. Moreover, the aspect ratio of the cones fabricated on the cross-linked polystyrene was nearly constant. The natural question arises, whether it is possible to control the aspect ratio by changing the surface properties? Or can we tune the height and width by changing exposure time and solvent concentration? Besides those, more technical questions, the mechanism behind the fabrication process also needs to be understood.

In my thesis, I tried to modify the surface of polystyrene to obtain different aspect ratios. Experiments were also conducted to monitor the growth of height and width of the cones in-situ. Both of the experiments provide indications about the mechanisms, which are also discussed.

1. 1 Atomic Force Microscope (AFM)

The Atomic Force Microscope (AFM), also known as Scanning Force Microscope, was invented by Binnig, Quate and Gerber in 1986 [14]. It is not only a microscope giving the researchers the topography of surfaces at atomic resolution or a device able to investigate physico-chemical properties of samples, but also a unique tool to structure and pattern of the surface of a material with nanometer precision.

1.1.1 General description of an AFM

A schematic representation of an AFM is showed in Figure 1.1. The working principle is the following: the sample is scanned by a tip mounted on a cantilever, which is fixed to a holder. The sample is moved by a piezoelectric scanner, which can move it along the vertical (z) and horizontal (x, y) directions. While scanning, the force between the tip and the sample is measured by monitoring a laser beam reflected off the backside of the cantilever. From that the information of the topography of the sample, or the interaction force between the tip and the sample, can be recorded and analyzed.

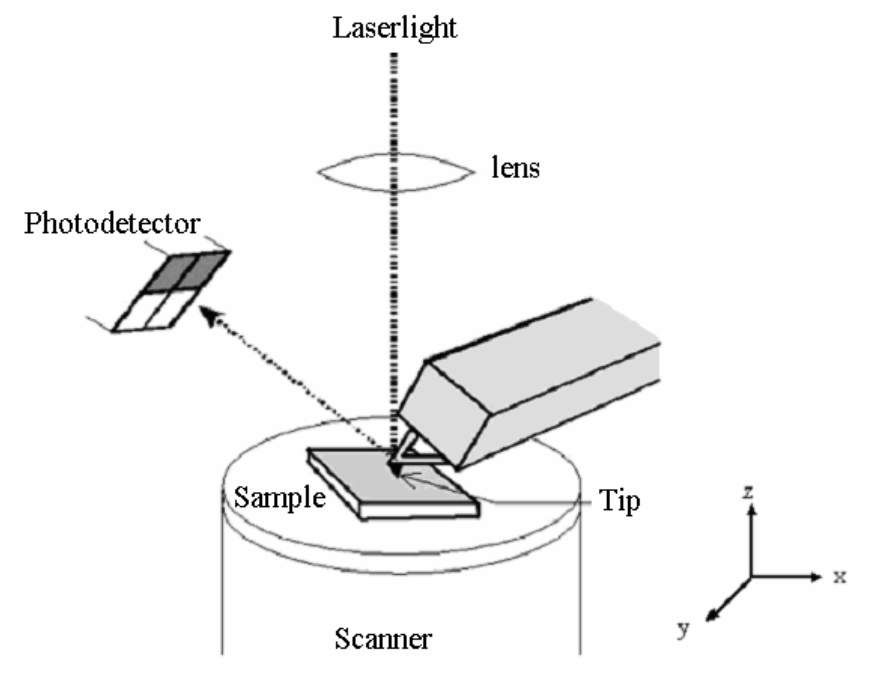

Figure 1.1 Schematic of an Atomic Force Microscope [15]

1.1.2 Imaging of surfaces

The AFM is most widely used for imaging the topography of surfaces. Depending on the type of the tips and/or sample, the AFM can be operated in several modes. Among there the tapping mode and contact mode are the most used.

In tapping mode the cantilever is oscillated around its resonance frequency. The oscillation amplitude is sensitive to the distance between tip and sample: when the tip is far away from the sample, the oscillation amplitude equals the free oscillation amplitude, which is usually between 20 and 100nm. As the distance between tip and sample are reduced, the tip touches the sample at each oscillation cycle and the oscillation amplitude is thus reduced. To keep constant oscillation amplitude, the piezoelectric scanner has to be extended or retracted according to the feedback loop during scanning. Then the vertical position of scanner at each (x, y) point will be recorded to obtain the topography of the sample. Tapping mode is applied mostly to soft samples, because the discontinuous contact of the tip with the sample protects the sample to be damaged.

In contact mode, the tip is always in contact with the surface. Instead of the oscillation amplitude of the cantilever, here the deflection is the main control parameter. The cantilever deflection is the measure of the force between the tip and the sample, and a feedback loop maintains it constant by vertically adjusting the scanner. During scanning in contact mode, soft samples can be damaged or some structures on the surface can be removed or destructed.

1.1.3 Force measurement

In addition to imaging the topography of a solid surface, AFM can also be used to record force-distance curves, which allow investigating the physico-chemical properties of a sample.

A force-distance curve is a plot of the cantilever deflection versus the piezo displacement, and consists of an approaching and of a retracting part. At the beginning of the approach

curve (step 1) the tip is so far away from the sample that there is no interaction in between. This part of the force-distance curve is called *Zero Line*. As the tip is approaching more and more (step 2) the attractive force [15, 16] is large enough to cause the tip to jump onto the sample. This discontinuity in the approach force distance curve is called *Jump-To Contact* and gives information about the attractive forces. After contacting the surface the tip continues pushing the sample (step 3), so the deflection of the laser will appear as being linear. This part is called *Contact Line*. When a maximum force is reached, the sample is withdrawn. At the beginning of the retract curve tip and sample are still in contact, and there is a *Second Contact-Line* which is observed during the step 4. The retract contact-line is always longer than the approach contact-line, because the adhesion forces act between the tip and the sample. The tip and sample detach (step 5), when the adhesion forces become smaller than the force exerted by the cantilever. The second discontinuity is called *Jump-Off- Contact*. Figure 1.2 shows the whole procedure of the measurement and the force curves before and after calibration.

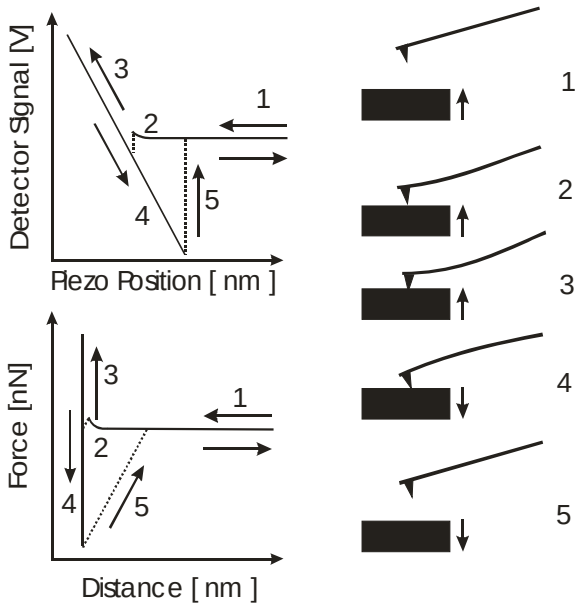

Figure 1.2 Force curves before and after calibration [16]

During the measurement, instead of measuring the deflection of cantilever and the real distance between the tip and the surface, we measure the voltage output by a photodiode

and the piezo displacement. After calibration of these data we obtain a force versus distance curve. Hooke's law is the key point to relate the force F and the deflection δ of the cantilever by the cantilever's spring constant k according to equation (1).

$$F=- k \delta \qquad (1)$$

The cantilever spring constant calibration is usually performed by one of the three commonly used methods: *Added mass method*, *Sader method* and *Reference spring method*. [17]

1.1.4 AFM based nanolithography

The working principle of AFM nanolithography is based on the interaction between the probe and substrate. When proper forces are exerted, and/or external fields applied, the probe can induce various physical and chemical processes on the substrate surface. Generally AFM based nanolithography can be classified into two groups: a) force-assisted AFM nanolithography, in which a force larger than that used in scanning is applied to the tip to produce mechanical indentation, plowing or pushing atoms and molecules; b) bias-assisted nanolithography, in which an external electric field in the range of 10^8V/m to 10^{10}V/m is applied to AFM tip and the tip acts as a nanoscale electrode.[1]

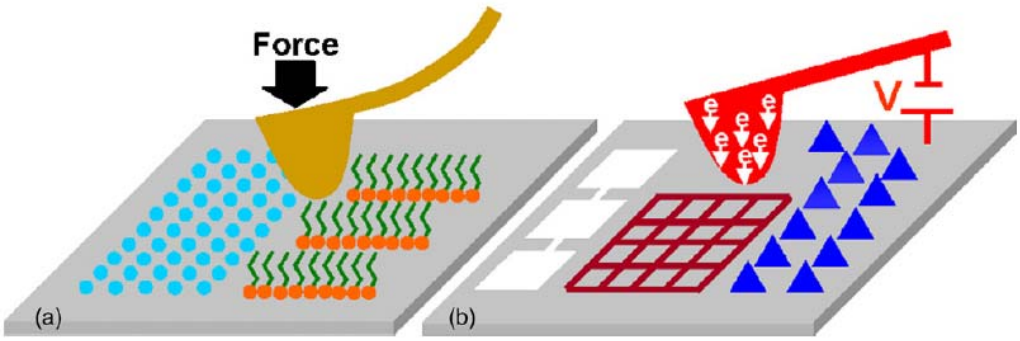

Fig 1.3 (a) Force-assisted and (b) bias-assisted AFM nanolithography. [1]

In force-assisted AFM nanolithography, indentation, static plowing and dynamic plowing are three typical methods. In indentation the tip is moved to a specific surface site, and indents the surface by applying large force. In static plowing, the tip is operated in contact mode, and scan across the surface along a predefined route with a large applied force. In dynamic plowing the tip is operated in tapping mode near its resonance frequency and the substrate is structured by increasing the modulation amplitude.

A number of papers on nanoindentation and dynamic plowing have been published by Cappella. [18, 19, 20] There is no fundamental difference between nanoindentation and dynamic plowing. [4] Only nanoindentation is a more time consuming method. During dynamic plowing, moreover polymer chain could be broken, which is revealed by the larger and softer border wall created during dynamic plowing. [18, 20]

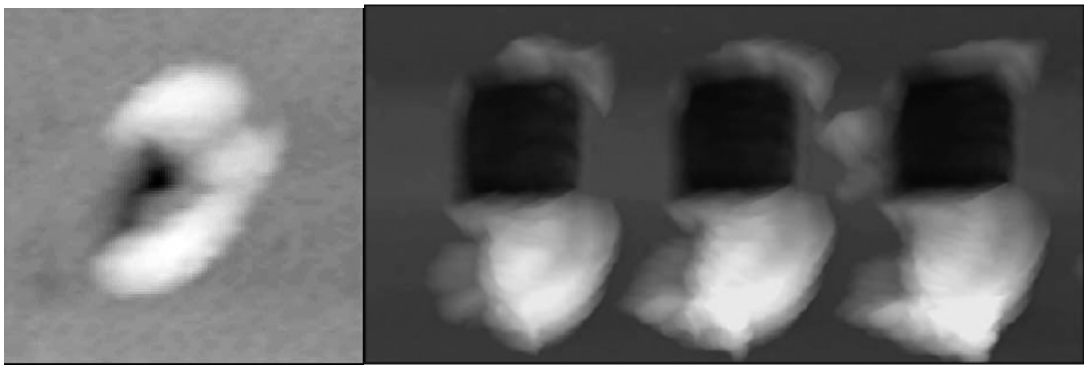

(a) (b)

Figure 1.4 (a) a single hole carved by AFM indentation on surface of Polymethyl methacrylate. The hole is surrounded by a pile-up wall which is called “border wall of a single hole”. (b) three squares carved on a surface of polystyrene through overlapping of single holes. [18]

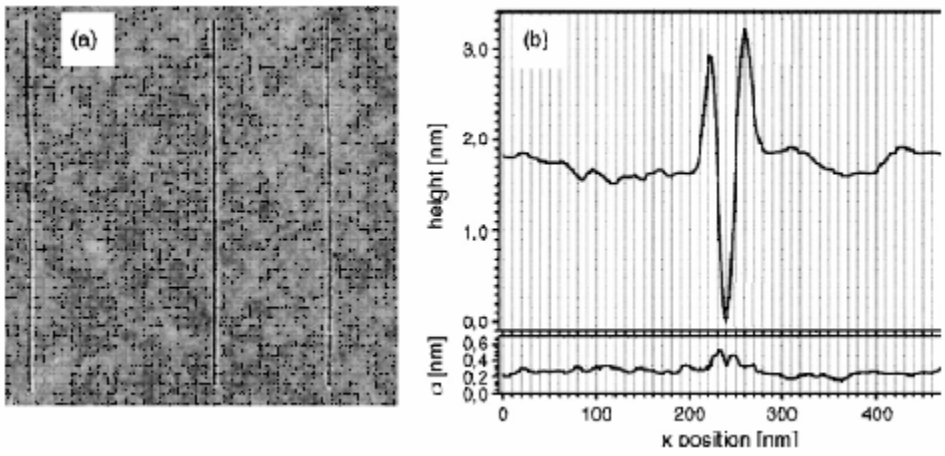

Figure 1.5 (a) three grooves created on PMMA. (b) averaged Z profile and its standard deviation. [19]

1.2 Plasma Treatment

Plasma is partially or wholly ionized gas with roughly equal numbers of negative and positive particles [21]. It is considered to be a distinct state of matter, apart from gas because of its unique properties [22].

Plasma treatment is probably the most versatile surface treatment technique for polymer and environment friendly [23, 24]. It is possible to choose different types of chemical modification for the polymer surfaces by choosing different gases. For example, oxygen-plasma can increase the surface energy of polymers, while fluorine-plasma can decrease surface energy of polymers and improves chemical inertness [25]. Inert gas plasma can introduce cross-linking at a polymer surface. The modification can be confined to the surface layer, up to several hundred angstroms without affecting the bulk properties of polymers. In the whole procedure no residual solvent, which must be used by wet chemical treatments will be introduced. The main disadvantage of using plasma is the requirement for the vacuum, which increases the cost of operation.

Reactions between gas plasmas and polymers can be classified in three groups: [26]

a) Surface reactions, which produce functional groups and cross-links to the polymer surface. These reactions include plasma treatment by argon, ammonia, carbon

monoxide, carbon dioxide, fluorine, hydrogen, nitrogen dioxide, oxygen and water.

b) Plasma polymerization, the formation of a thin film onto the surface of a polymer by polymerization of an organic monomer, with gases such as such as CH_4, C_2H_6, C_2F_4, or C_3F_6.
c) Etching (physical etching and chemical etching) to remove the materials from a polymer surface. Oxygen plasma and oxygen- and fluorine- containing plasmas are frequently used for this procedure.

1.3 Sputtering Deposition

Sputtering deposition is physical vapor deposition (PVD) method of depositing a thin film of material, called target, onto a substrate. The atoms of the coating material are ejected from the surface of the "target" by ions accelerated under a high voltage in vacuum. The atoms not in their thermodynamic equilibrium state and tend to deposit on all surfaces. A substrate is placed in the sputtering chamber and is coated with a thin, firmly bonded film. Sputtering usually uses argon plasma, and is used in semiconductor industry for coating substrates with thin films of electrically conductive or non-conductive materials. [27]

1.4 Self-Assembled Monolayer of Thiolates on gold

Bare surfaces of metals and metal oxides have the tendency to adsorb adventitious organic material in order to reduce the free energy of the interface between the metal or metal oxide and the ambient environment. [28] Self-Assembled Monolayers (SAMs) are organic assemblies adsorbed on metal or metal oxide surfaces, from solution or from the gas phase. There are three types: alkanethiols ($HS(CH_2)_nX$), dialkyl disulfides (X(CH2)*m*S-S(CH2)*n*X), and dialkylsulfides (X(CH2)*m*S(CH2)*n*X), where *n* and *m* are the number of methylene units and X represents the end group of the alkyl chain (-CH3, -OH, -COOH). SAMs provide a convenient, flexible and simple system to alter interfacial properties and stabilize nanostructures of metals and metal oxides. [29] SAMs have a chemical functionality (head group) with a specific affinity for a substrate. They organize

spontaneously into well-ordered, close-packed structures on the surface. The end group of the adsorbate determines the surface properties.

gold is the standard substrate [30] and widely studied. gold is easily obtained and straightforwardly prepared by PVD, sputtering, or by electrodeposition. Its inertness also makes it a good choice as a substrate for studying SAMs.

The central bonding habit of the high-coverage thiol phases on Au (111) is generally accepted.[30,31,32,33] The alkanethiols are arranged in a $\sqrt{3}\times\sqrt{3}$ R30 structure, with a tilt angle of 30° from the surface normal.[33,34] The chemisorption of either thiols or dialkyl disulfides on the Au (111) surface gives Au+-thiolate (RS-) and releases H_2. [35]

$$Au_n^0 + RSH \rightarrow \left[RSAu^{2+}H^-\right]\cdot Au_n \rightarrow RS^-Au^+\cdot Au_n + \frac{1}{2}H_2$$

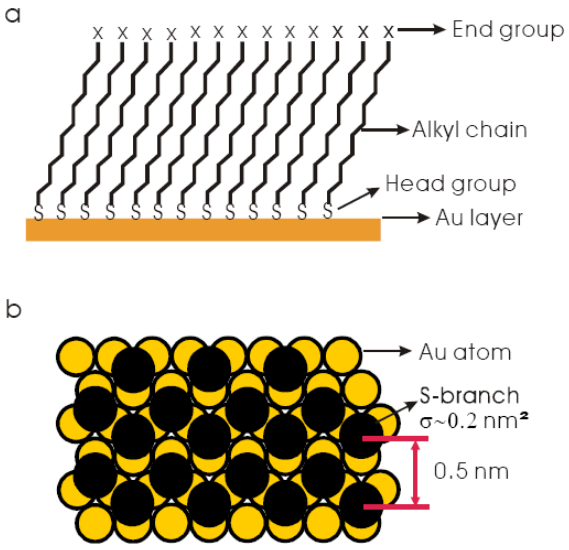

Figure 1.6 Schematic diagram of arrangement of thiolates on Au (111) lattice. (a) Profile of the SAM. X represents the end group, which can be -CH_3, -OH, -NH_2, etc. The tilt angle of the alkyl chains is 30°. (b) Thiolates on Au surface are arranged as a33×R30°. The sulfur atoms are positioned in the 3-fold hollows of the Au lattice. σ is the area of the cross section of an alkyl chain. [36]

2. Experiment and Setup

2.1 Ex-situ experiments

Commercial 1.2mm thick polystyrene plates (Goodfellow Ltd, HμNtingdon, England) were used as substrates. Their molar mass has a broad distribution (mean number Mn = 150kDa, mean weight Mw = 310kDa, and PDI (poly dispersity index) = 2.07).

First, the polystyrene plate was cleaned in methanol in an ultrasonic bath (Super RK 156BH) for 4mins. Afterwards, it was put into argon plasma with pressure of 0.5mbar in a plasma generator of the type 'Femto' (Diener Electronic, Nagold, Germany) with the power 60W for 4mins to introduce crosslink to the superficial layer of polystyrene. After crosslinking, polystyrene was cleaned in the methanol ultrasonic bath again.

The sample was scanned by an atomic force microscopy (Nanowizard, JPK, Berlin) in tapping mode. A tapping mode tip (OMCLAC 160 TS-W silicon) with a spring constant of 42N/m was used. The sensitivity of the cantilever was calibrated before experiment every time. In the force mapping mode a large force between 16μN and 24μN was applied onto the tip to indent the polystyrene surface. After indentation, the sample was placed in a closed vessel. This vessel contained a piece of filter paper soaked with toluene solution, which easily evaporates. When the vessel was closed, it will be saturated with toluene vapor that penetrated both the cross-linked superficial and the non-cross-linked underlying polystyrene. After a certain time, the sample was taken out and imaged in tapping mode by JPK again.

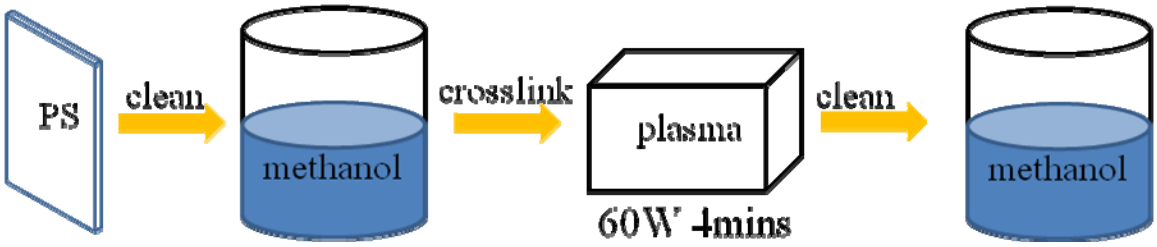

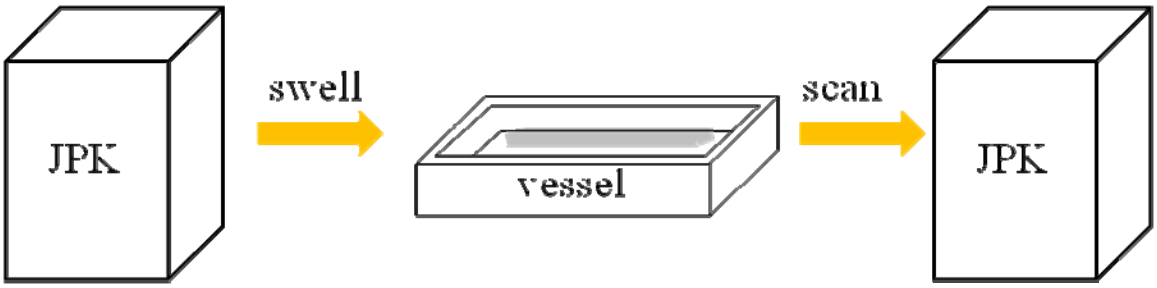

Figure 2.1 Procedure of treatment to polystyrene plates

2.1.1 Preparation of SAMs on gold-PS substrate

Chemicals

Methanol, HPLC, Merck, Darmstadt, Germany

1-Dodecanethiol 98%, Sigma-Aldrich Chemie Steinheim Germany

11-mercapto-μNdecanol, 97%, Aldrich, Germany

11-Amino-1-1μNdecanethiol

gold 99.9%

Au (111) surface was prepared by sputtering (BALTEC MED 020 Coating System, BALTEC, Witten/Buhr, Germany) onto freshly cleaned polystyrene substrates. The pressure of argon was 5×10^{-2} mbar. After sputtering, the substrates were immersed into 1mM methanolic SAM solutions for an hour. Then they were rinsed by methanol and dried in the hood.

2.2 Setup for in-situ experiments

The JPK Instruments NanoWizard™ Atomic Force Microscope (AFM) was used. The AFM head is installed on an inverted optical microscope made by Zeiss. The light source is from the top. Samples are placed on a stage, which can also be heated up. Sensor and cantilever are installed in the AFM head. A stabilization table under optic microscope is used to reduce acoustic noises or disturbances from the environment.

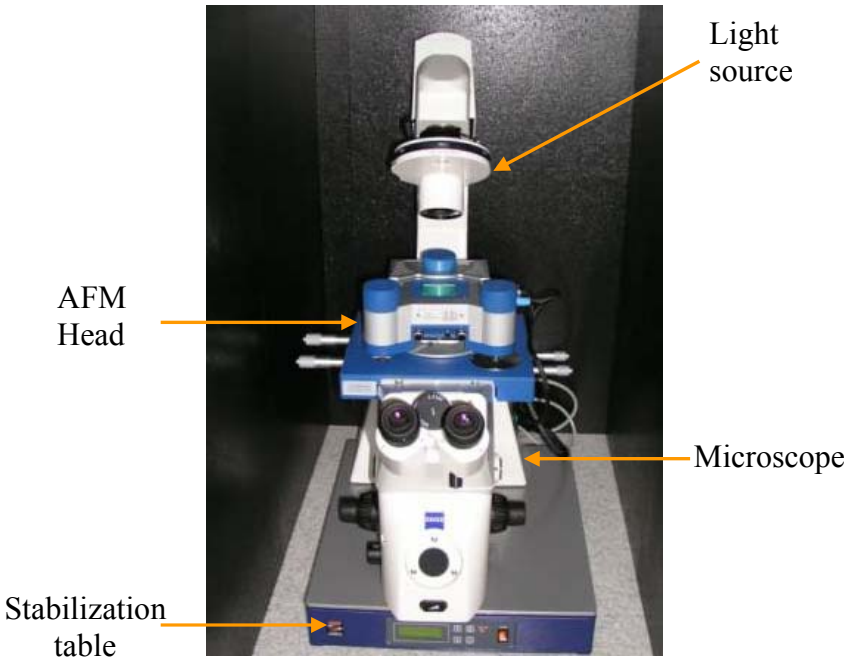

Figure 2.2 JPK instrument

Samples can be scanned in the air, vapor or liquid. When scanning in the vapor or liquid, the cantilever is clamped to a special glass block cantilever holder, which is locked into the AFM head. An O ring is needed to seal the space between cantilever and sample. There are two holes in the glass block, to let the vapor and liquid in and out.

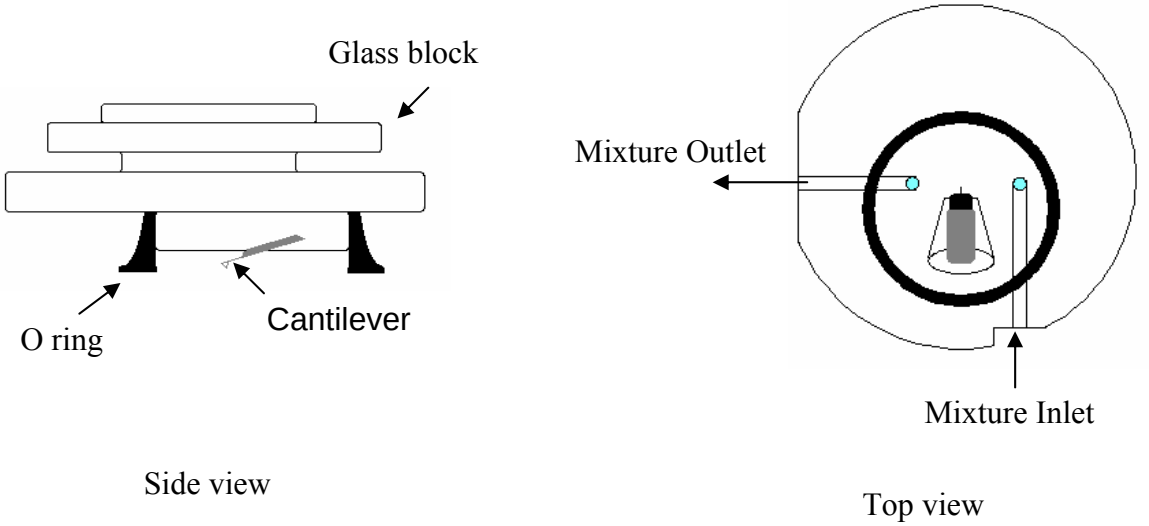

Figure 2.3 Glass block cantilever holder

2.3 Gas mass flowing control for the in-situ experiment

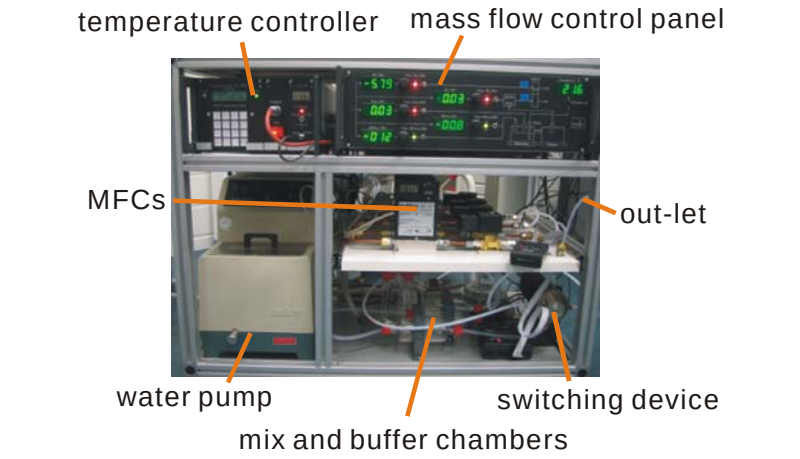

(a)

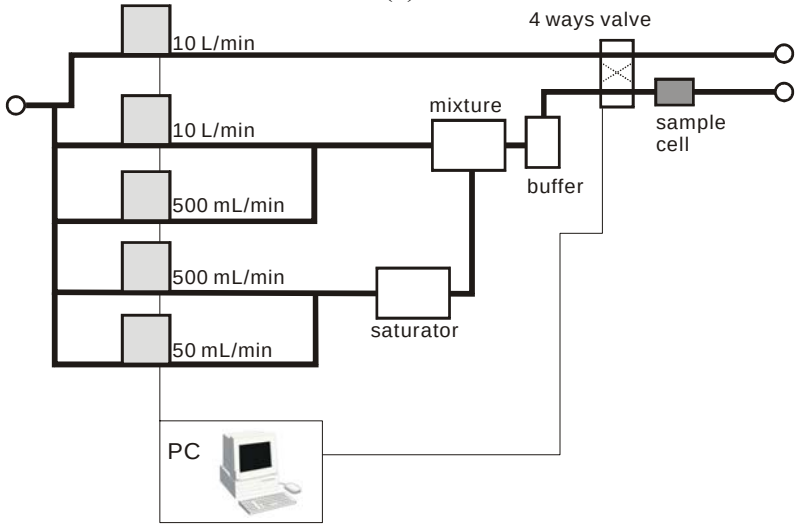

(b)

Figure 2.4 schematic of gas flowing system. (a) component of gas flowing system. (b) gas lines of gas flowing system.

The concentration of toluene vapor mixed to pure nitrogen gas flow is controlled by a gas flowing system designed by Dr. Masaya Toda. 5 mass flow controllers (MFCs) are installed. They are controlled by a PC. There are mainly two gas flow lines. One is a nitrogen gas flow line which is controlled by a max 10L/minute MFC. The other line is used for the vapor flow. Vapor concentration is controlled by the other four MFCs (max 10L/min, 2x 500ml/min and 50ml/min). Every main line is connected to a two ways electrical switching device, which can exchange the inlet and outlet in one second.

To create controlled toluene vapor flow, smaller MFCs (max 500ml/min and 50ml/min) control flow mass of two lines which pass through the saturator chamber, a toluene solvent container. These lines are connected to the other two lines for nitrogen flow which is controlled by the other MFCs (max 10l/min and max 500ml/min) at the mixture chamber. The vapor concentration is controlled by controlling the flow ratio of saturated vapor and nitrogen gas into the mixture chamber. An extra buffer chamber of 100ml is fixed between the mixture chamber and the switch device to escape the impact of switching gas lines.

At 22˚C the pressure of saturated vapor of toluene is 33kPa. Therefore the concentration of toluene in saturated nitrogen vapor is approx 3000000ppm at atmospheric pressure.

3 Results and Discussion

3.1 Ex-situ experiments

Argon plasma treatment produced cross-linking effect to the superficial layer of polymers. [21] It is known that cross-linking affects the stiffness of polymers. [37] Cappella et al. investigated this effect on polystyrene. The cross-linked layer has a larger Young's modulus than the untreated, original polystyrene, [38] so the polystyrene surface can not be indented very deep by an AFM tip even with a large force applied. [38-41] The stiffness and the depth of the superficial cross-linked layer are influenced by time and power of the plasma treatment. [13] Stripes, star-like morphologies or pinnacles could be generated when exposing polystyrene with low crosslinking degree into organic solvents (liquid or vapor phase). [39]

To avoid these effects due to insufficient crosslinking, plasma treatment should be strong enough. Polystyrene in Figure 3.1 was treated by plasma for 4mins with 60W. The whole treatment was the same as described in 2.1. The following images showed the surfaces of polystyrene after crosslinking, (a), indentation (b) and swelling (c). The scan area is 60x60μm^2. The scratch on the surface of polystyrene (see arrows) remained the same after swelling for 30s. So in the following experiment plasma power and time I chose were 60W and 4mins throughout.

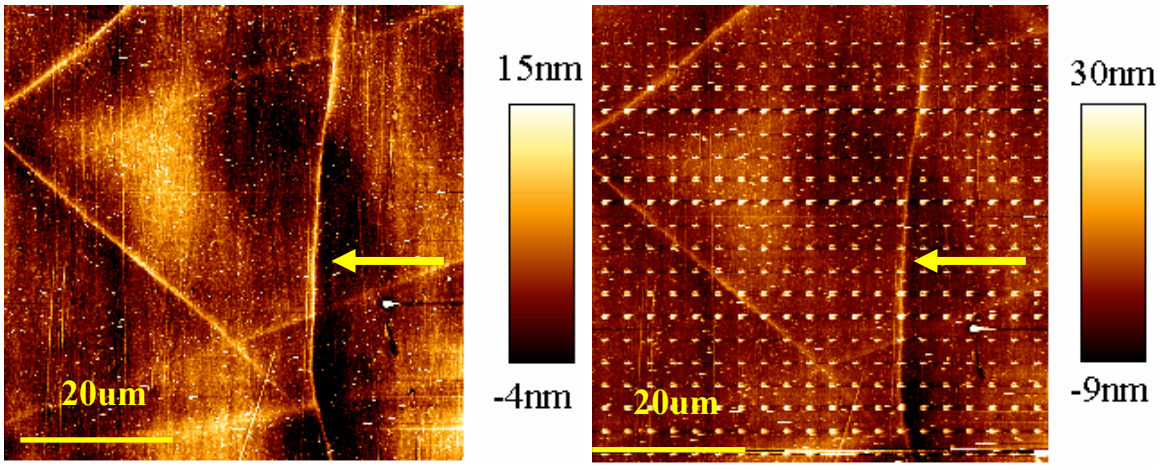

(a) (b)

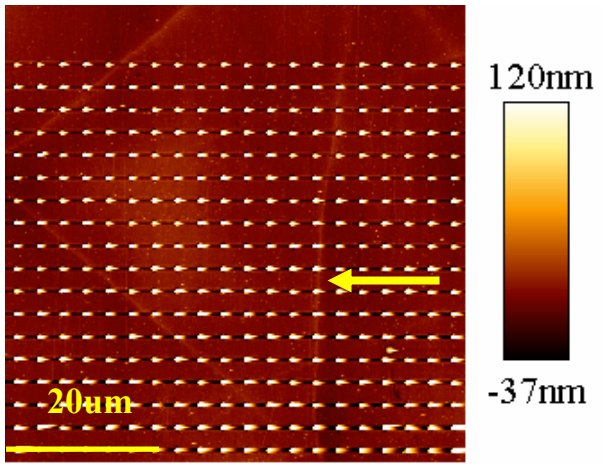

(c)

Figure 3.1 AFM tapping mode image of polystyrene surface after crosslinking (a), indentation (b) and swelling (c).

The images in Figure 3.2 show the holes after indentation (a) and cones after swelling (b) in small scale. A large border wall around the holes is observed in (a). The volume of the material out of the surface should be equal to the volume of the hole. The holes we observe are not as large and deep as we expected. This is due to the convolution effect which is introduced when the samples have features that are on the same size as the probe tip used for image during scanning. [42] In (b) a concentric depression along the rim of the cones suggests that a displacement of the non-cross-linked material underneath the cross-linked surface layer takes place.

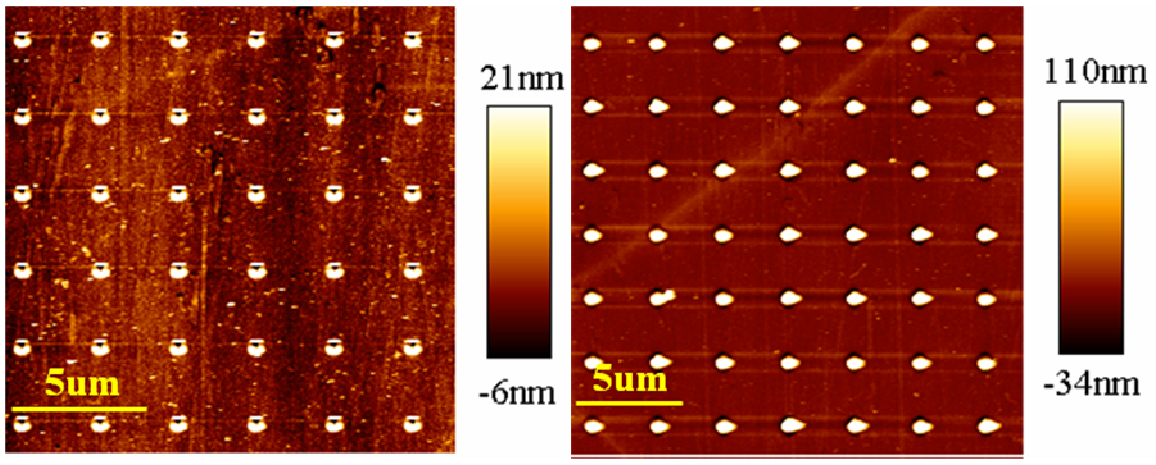

(a) (b)

Figure 3.2 Tapping mode images of polystyrene surface in scale of 20μm after indentation (a) and swelling (b). Note the different Z scale of (a) and (b)

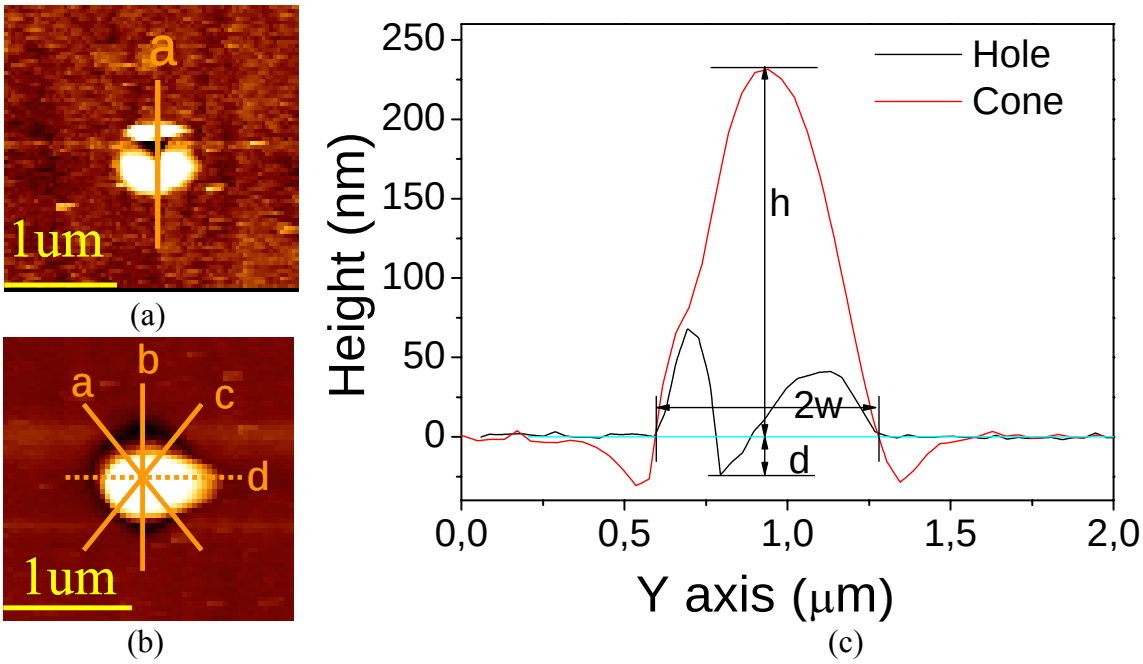

Figure 3.3 Single images of a hole (a) after indentation and a cone (b) after swelling. (c) Schematics for definition of depth, width and height.

To calculate the aspect ratio, height and width were defined as shown in Figure 3.3 (c). In cones, profiles are cut from three directions to obtain average values because of the asymmetry of the cones, which is probably due to the initial asymmetry of the holes. The height is the value of the highest point. To define the width, we define a base-line (the blue line) in stand of the surface. The width (w) of cone is defined as the distance between the two contact points with the baseline. The aspect ratio (α) is defined by the equation (2). For holes, the most important parameter is the depth, which states the initial conditions. A profile is taken in 'a' direction and the deepest point is read as the depth.

$$\alpha = \frac{h}{w} \qquad (2)$$

Two samples which were treated as described in 2.1 are analyzed. Results are shown in Figure 3.4: the aspect ratios of two samples are 0.50 and 0.64, respectively. Initial depth of sample 1 is 10nm. After swelling for 60s, the cones grew to 172nm with aspect ratio of 0.5. For sample 2, the depth is 27nm. After swelling for 30s the cones grew to 224nm with 0.64 of aspect ratio. The results show that a lower depth leads to a lower structure with a smaller aspect ratio.

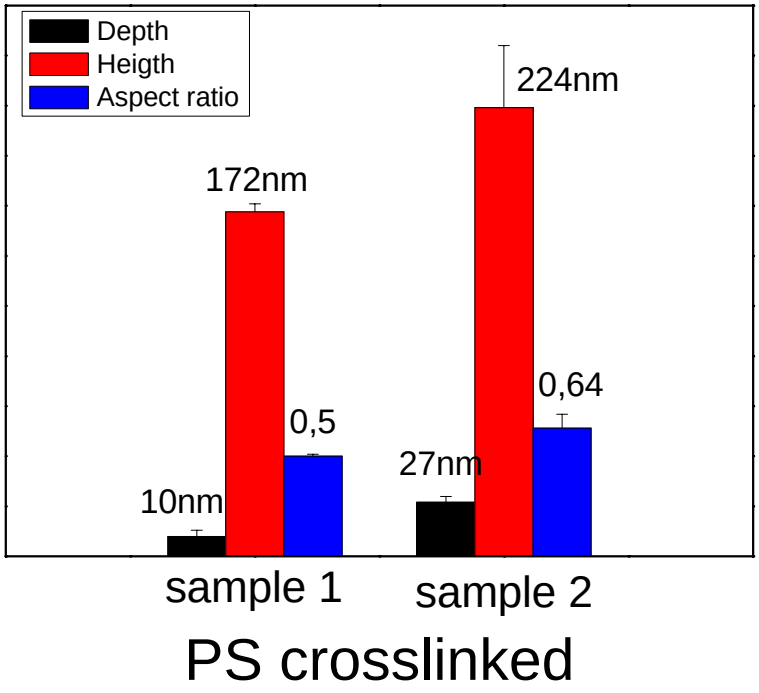

Figure 3.4 Two samples from ex-situ system

3.2 PS surface modification

To obtain a structure with a high aspect ratio, we need to find out the mechanism behind the structure formation. The whole procedure is mainly depending on the mechanical properties of the superficial cross-linked layer and on the swelling behavior of polystyrene. We propose two mechanisms to describe this process: a) flowing mechanism and b) swelling mechanism.

1) Flowing mechanism: under the cross-linked layer, the non-cross-linked material swells and flows out to the surface through holes. In this mechanism, the "squeezing out" material leads to a mostly vertical growth. A depression at the rim may be left behind.

2) Swelling mechanism: the indention breaks the network of the cross-linked layer. Toluene vapor penetrates into polystyrene. The non-cross-linked polystyrene swells, and the superficial cross-linked layer deforms. Then the whole surface swells. This leads to a lateral expansion of the cones.

(a) flowing mechanism (b) swelling mechanism

Figure 3.5 two possible mechanisms

In the flowing mechanism, surface properties would affect the aspect ratio due to the different contact angles forming on different surfaces during the process of cone formation. In swelling mechanism, the surface properties would not make difference for the aspect ratio. To figure out the actual mechanism, I modified the polystyrene surfaces.

3.2.1 Contact angle measurement

Before surface modification, I chose three different thiolates to compare the contact angles of polystyrene solutions on the thiol modified surfaces.

Contact angle measurements were carried out onto a silicon surface with a sputtered gold layer and adsorbed thiols. Three solutions were tested: water and two different concentrations of polystyrene. Water is ultraclean water. PS powder was diluted by toluene to a mass concentration of 1% and 0.1%. Three agents, 1-Dodecanethiol, 11-Mercapto-1-undecanol and 11-Amino-1-undecanethiol were diluted to 1mM by ethanol. The thoil solutions were freshly prepared before experiment

Table 1. Contact angle measurement result /°

solution	**-OH**	**-NH_2**	**-CH_3**
H_2O	41,5	56,2	**107,9**
1% PS	3,6~4,1	2,1~2,3	**42,7**
0.1% PS	2,4~3,4	5,6	**43,7**

In Table 1, the contact angle of water on the surface with the end group of CH_3 is 108˚, the largest for three thiols. And so is the contact angle of polystyrene solutions. The end group of CH_3 provides the surface with the lowest surface energy, so I chose 1-Dodecanethiol as the agent.

3.2.2 Surface modification system

I) PS-Au-CH_3 system

To attach the thiol, a 20nm thick gold layer was sputtered on to the surface of polystyrene. After that the whole sample was immerged into the thiol solution for 1hour and dried in a hood. Then the sample was imaged and indented with the AFM. After exposing to toluene vapor, the structures formed and were imaged by AFM. This system is called PS-20nmAu-CH_3.

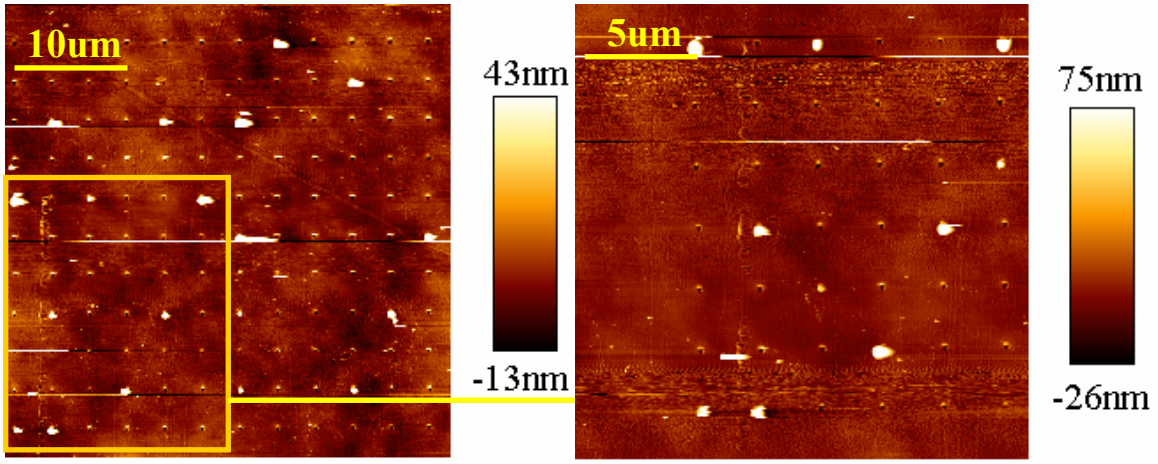

(a) 120s (b) 240s

Figure 3.6 Image of PS-Au-CH_3 after swelling 120s (a) and 240s (b)

In system I), indentation force loads were 16μN and 24μN. After exposing to toluene vapor for 120s only a few structures were formed from holes produced by 24μN force load. These cones have a large height distribution from 80 to 160nm. Then the sample was put into toluene vapor for another 120s. No further cones grew, but height increased by 10%, and so did the aspect ratio. Average and standard derivation of height, width and aspect ratio are shown in Table 2.

Table 2 Information of PS-Au-CH_3 system

system	Au layer thickness	Indentation		swelling			
		force load	depth	time	height	width	aspect ratio
PS-Au-CH3	20nm	24μN	62±12	120s	130±29	417±42	0,31±0,05
				120+120s	142±23	433±43	0,33±0,04
		16μN	40±6	120	No cones grew		
				120+120s			

The holes indented by 16μN force and the most of the holes indented by 24μN force remained the same (no growth of cones was observed). This means that the force is too low or the thickness of the gold layer is too thick for AFM tip to break through. There are two possible reasons for the fact that the system worked partially for some holes which is indented by 24μN force load only. One can be due to some defects in the gold layer during sputtering. Cantilevers can easier go through the gold layer where defects were. The other one could be due to the immersion in the thiol solution. Part of the gold might be washed away by the solution.

Compared to the cross-linked polystyrene (PSc) system, the aspect ratio and the height of the structures from PS-20nmAu-CH_3 are lower. Uncertain of the surface in this system makes this result meaningless, so several systems were developed in the following experiments.

II) PS-Au system with different thick gold layers

In system I), partially working means that gold layer is too thick. So I tried to reduce the thickness to find the proper thickness by which I can obtain nano structures. I chose four different thicknesses: 20nm, 16nm, 10nm and 6nm.

Different thick gold layers were sputtered onto the surfaces of the polystyrene. Without attachment of thiol, the samples were indented and imaged by AFM. After exposed into solvent, the samples were scanned by AFM to obtain the topography.

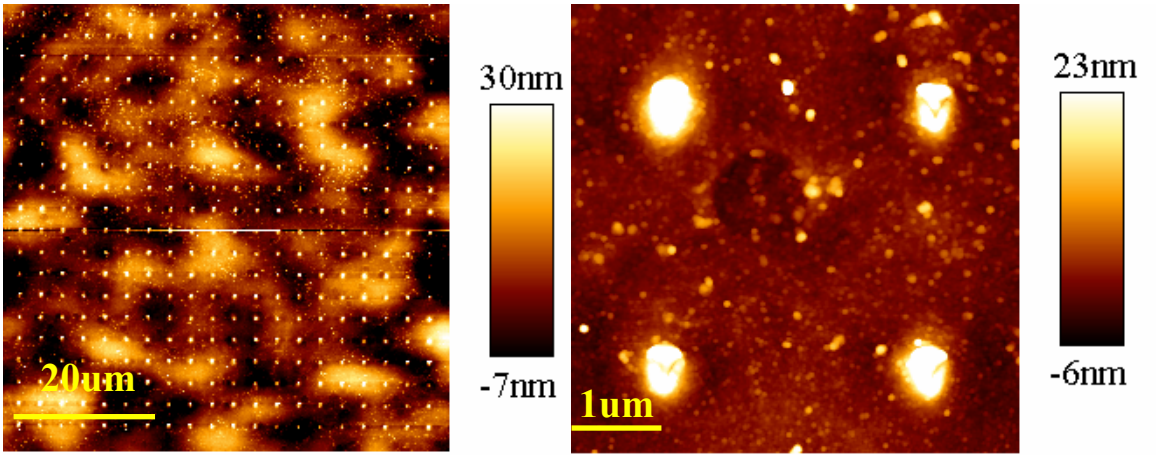

(a) 10nm (b) 10nm

Figure 3.7 PS with 10nm Au layer

The 20nm gold layer is too thick for AFM to break through: no cones grew after exposure to toluene vapor for 120s, and the holes remained unchanged. The 6nm gold layer was too thin to protect the polystyrene surface from swelling, the whole surface swelled. 16nm gold layer and 10nm gold layer (Figure 3.7) worked: cones grew, but on the top of the cones, indented holes still can be seen. The reason is that the height of the grown structures is only between 50 and 60nm, which is much lower than that in the previous experiments. And the aspect ratios of two systems are lower than 0.2.

III) PSc-6nmAu system

Although in PS-10nmAu and PS-16nmAu systems structures formed, the height and the aspect ratio of these structures are extremely small. Since the 6nm thick gold layer cannot protect the polystyrene surface from swelling, but allow to change the surface properties of polystyrene via functionalization with SAMs, I sputtered 6nm gold onto the surface of the cross-linked polystyrene.

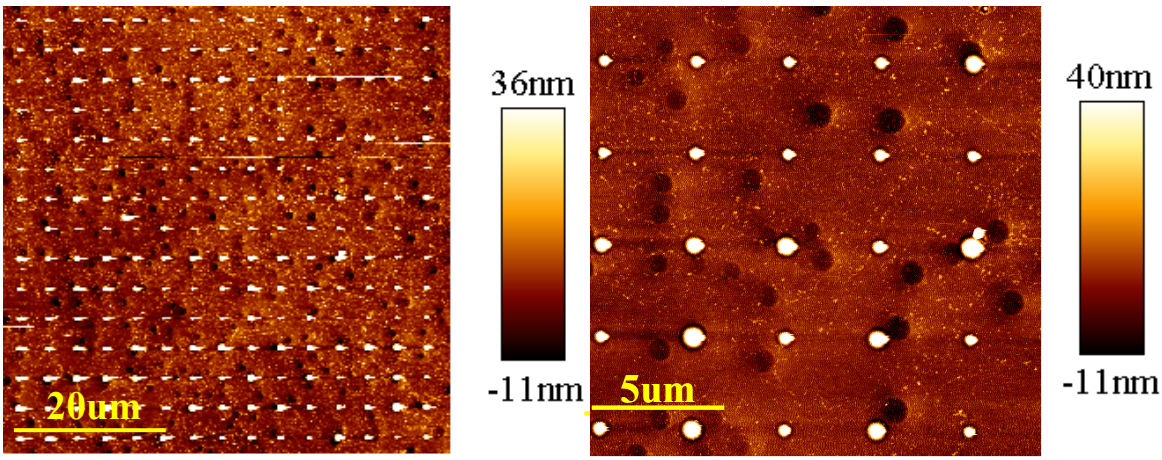

(a) 60s (b) 60s

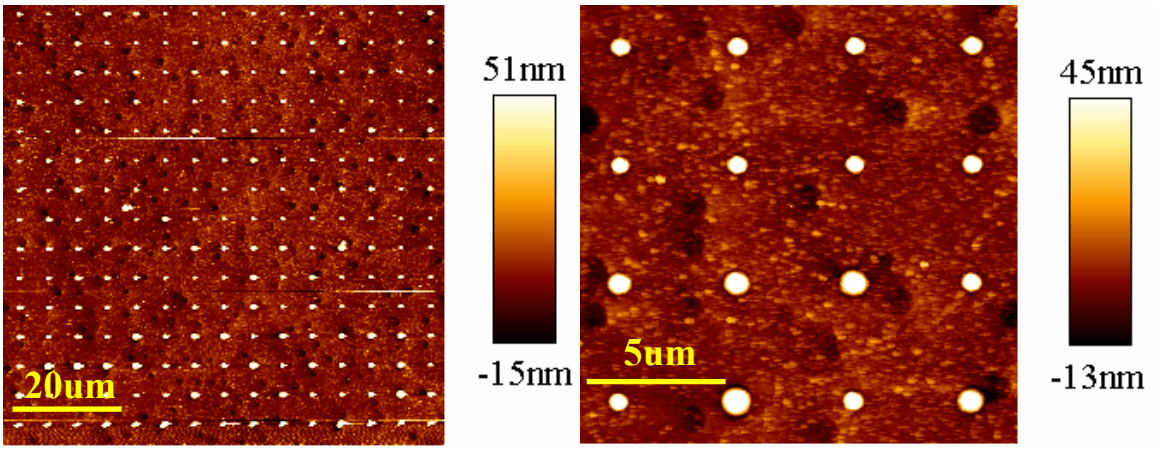

(c) 60+60s (d) 60+60s

Figure 3.8 PSc-Au exposing into toluene solvent for 60s (a), large scale, and (b), small scale; for120s (c), large scale and (d), small scale

The sample was exposed to the solvent vapor twice, 60s each time. The cones grew, but not as uniform as those in PSc system or PS-Au system. The depression at the rim is the same as in the PSc system. Depth, height and width are summarized in Table 3. After the second swelling, the height was 126nm which is lower than 137nm, the width was 377nm which is larger than 352nm, and the aspect ratio was lower: it changed from 0.39 to 0.33.

There is a possible explanation for the fact that the aspect ratio was lower after longer exposure time to toluene vapor: the cones reached saturation and collapsed， which was also observed in previous study [13].

Table 3 Information of PSc-Au system

system	thickness	indentation		swelling			
		force load/μN	depth/nm	time/s	height/nm	width/nm	aspect ratio
PSc-Au	Au:6nm	24	17±6	60	137±28	352±65	0,39±0,04
				60+60	126±21	377±53	0,33±0,02

IV) PSc-Ti-Au-(CH_3) system

System III), the PSc-6nmAu system, demonstrated that combining a 6nm gold layer and cross-linked polystyrene can protect the surface from swelling. The superficial gold layer can be used to change the surface properties by a SAM. So in this step I tried to attach thiol onto the surface. Since a 6nm gold layer is too easily washed away, especially when immerged into the thiol solution, I sputtered a 2nm titanium layer before sputtering the gold layer. This enhances adhesion of gold on the surface. Then samples were immerged in the thiol solution for 1hour.

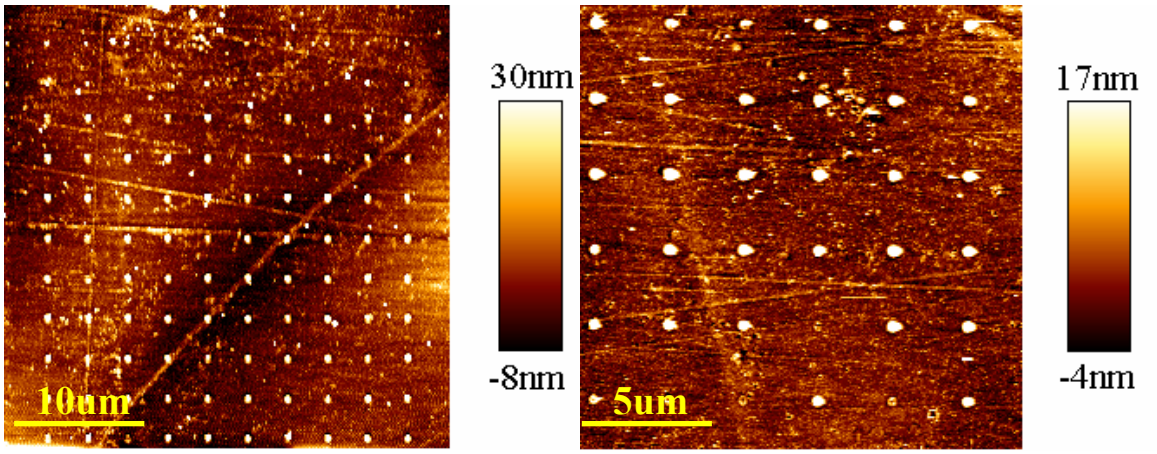

PSc-2nmTi-6nmAu 60+60s PSc-2nmTi-6nmAu-CH3 120s

Figure 3.9 PSc-Ti-Au with and without CH_3 terminated thiols swelling for 120s

PSc-2nm-Ti-6nmAu and PSc-2nmTi-6nmAu-CH_3 systems worked as shown in Figure 3.9. After exposed to toluene vapor for 2 minutes, the height only reached 40~70nm. The aspect ratio was between 0.1 and 0.2. (Table 4) The presence of the titanium layer caused a significant decrease on the aspect ratio and height of the structures. There are no available data in PSc-Ti-Au-CH_3 system for swelling 60s, because even through there were cones, the lower structures made it difficult to detect.

Table 4 information of PSc-Ti-Au/CH_3 system

system	thickness	Indentation		swelling			
		force load/uN	depth/nm	time/s	height/nm	width/nm	aspect ratio
PSc-Ti-Au	Au:6 nm Ti:2nm	25	20±3	60s+60	63±6	366±16	0,17±0,02
		20	18±4				
PSc-Ti-Au-CH3	Au:6nm Ti:2nm	24	24±5	60	No data are available		
				120	42±7	286±37	0,14±0,02

3.2.3 Result of the ex-situ experiments

There are two possible mechanisms for this process: flowing mechanism and swelling mechanism. If the process is dominated by the flowing mechanism, the surfaces with the same surface energy should provide the same aspect ratio. While if the process is controlled by the swelling mechanism, the surface properties would make no difference for the aspect ratio. After analyzing the four surface modified systems, I compare the obtained aspect ratios and heights with each other. (Figure 3.10)

The highest aspect ratio is from system I) PSc system and equals to 0.6. The second highest aspect ratio is between 0.3 and 0.4, and was obtained from PS-Au-CH3 and PSc-Au. The lowest aspect ratio is between 0.1 and 0.2, and was from PS-Au, PSc-Ti-Au-CH_3 and PSc-Ti-Au systems.

The PSc system has the aspect ratio of 0.6. The aspect ratios of the systems with CH_3 termination group on the surfaces, PS-20nmAu-CH3 and PSc-2nmTi-6nmAu-CH_3 systems are 0.33 and 0.14 respectively. In the systems with gold surface, PS-10nmAu, PS-16nmAu, and PSc-6nmAu, and PSc-2nmTi-6nmAu systems, the aspect ratios are 0.18, 0.17, 0.39 and 0.17. In other words, the same surface did not lead to the same aspect ratio as we expected. This phenomenon implies the mechanism of this process may be swelling, but not flowing.

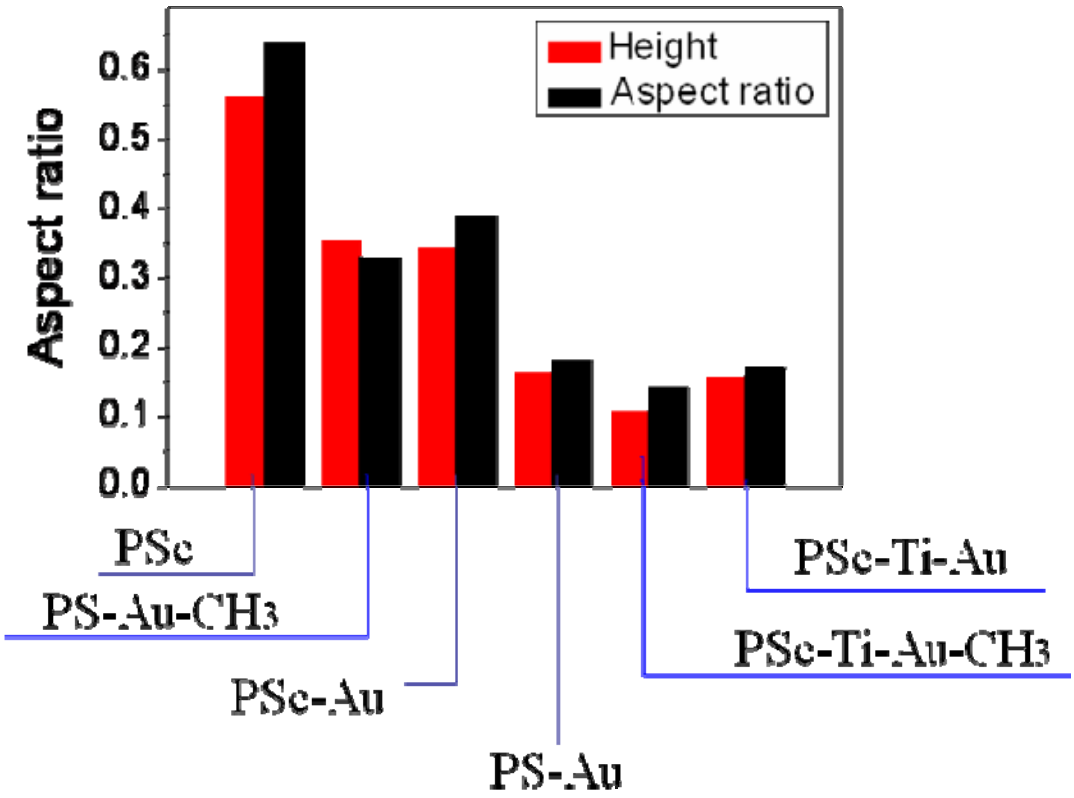

Figure 3.10 Comparison of different the aspect ratios and heights obtained in the four systems

It is however too early to draw a conclusion. Since another important factor needs to be taken into account: the kinetics of the swelling process. As we can see from Figure 3.10, the structures with lower aspect ratios also have lower heights.

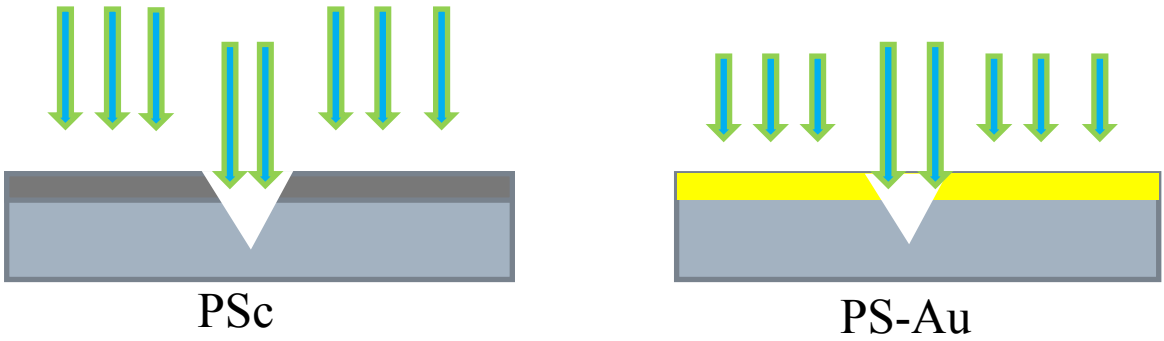

Figure 3.11 schemes of toluene vapor penetrating the polystyrene surface

It must be pointed out that in the PSc system, the cross-linked polystyrene layer can protect the non-cross-linked polystyrene underneath from swelling, but it can not stop the toluene vapor from penetrating into the polystyrene. In the PS-Au system it is a different case. If the thickness of the gold layer is larger than around 10nm, then it is not possible for the toluene vapor to go through the gold layer. This will slow down the whole swelling process, and so also the growth of the nanostructures.

As shown in Figure 3.12, the PSc system gave the highest aspect ratio. The thin gold layer in the PSc-6nmAu leads to the second high aspect ratio. The systems with the thick gold layer and the titanium layer in between provide the lowest aspect ratio. So a kinetics study seems to be important to figure out the mechanism behind the structures formation and the different aspect ratios.

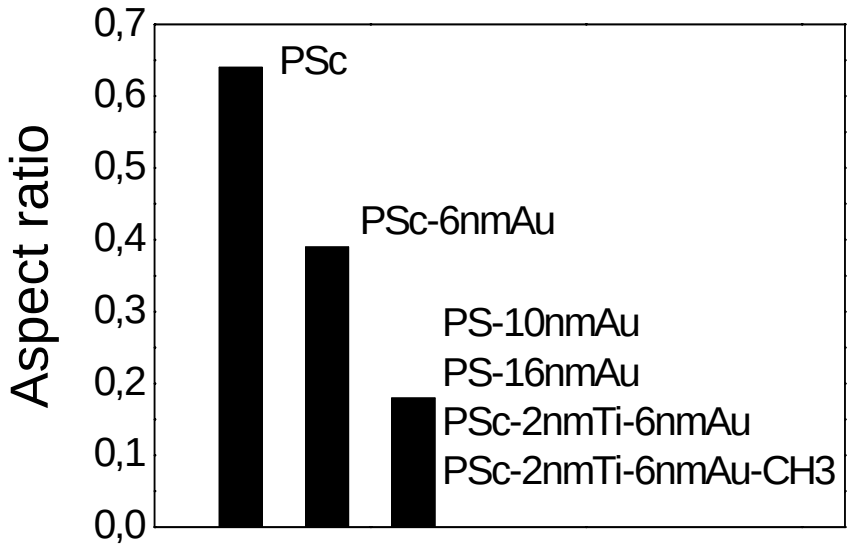

Figure 3.12 compare aspect ratios of different superficial layers

3.3 In-situ System

In the ex-situ experiments, different samples could hardly be compared to each other because of the kinetics involved. To study the kinetics, I chose the in-situ system.

All polystyrene plates used in this experimental part were treated by plasma for 4mins with power of 60W, the same as in the ex-situ system. The difference between the ex-situ experiments is that samples were not taken out of the AFM cell to be exposed to toluene vapor, but the treatment was done inside the AFM cell.

To monitor the samples during swelling, the space between the sample and the glass block was sealed by an O-ring, which can prevent toluene from leaking. The concentration of toluene is controlled by a gas mass flow control setup. It went into the cell from inlet hole on the glass block, which is connect to the outlet of gas mass flow control setup by a Teflon tube. The exhaust gas was expelled from the outlet tubing on the glass block. It passed a buffer which contained molecular sieves, then was vacuumed by a vent.

3.3.1 45% toluene concentration and 24μN force load indentation

When the relative toluene concentration in nitrogen was ever below 45%, no cones were observed. Figure 3.13 shows the topography images acquired when relative concentration of toluene is 45%; the force load during indentation is 24μN. The depth of the holes is 100nm. 20.8mins were needed to take one picture. First, only nitrogen gas passed through the system. The sample was scanned and indented under nitrogen (a). From the yellow line in (b), nitrogen was switched to the mixture of toluene and nitrogen. Then structures started growing (b), (c). Scanning proceeded during the growing. The yellow arrow lines show the direction of time during scanning, and the scan rate is kept constant. So we can calculate the time that the sample is exposed to the toluene mixture by calculating the distance from the beginning of the scan. After a certain time, the cones stopped growing. At this point the mixture of toluene and nitrogen was switched to nitrogen again (d). The scanning continued for another 20 minutes.

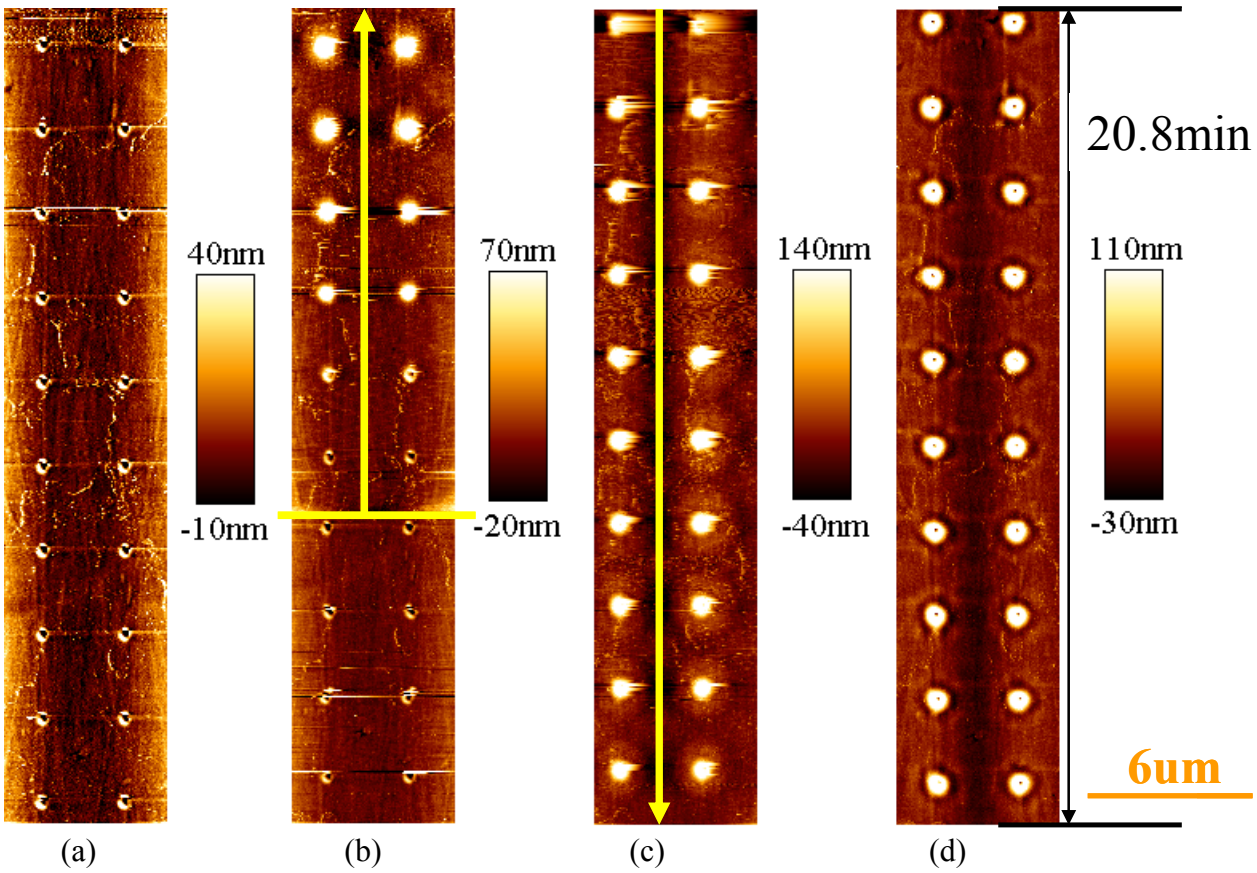

Figure 3.13 In-situ systems with 45% toluene and 24μN indentation force load. (a) image after indentation under nitrogen. b), c) from the yellow line, toluene vapor was put in, and the arrow shows scan direction (the time axis). d) Picture taken after toluene stopped flowing.

When toluene vapor was injected (from yellow line in (b)), the cones started growing both in width and height dramatically during the first 10 minutes. In the following 20 minutes, there was no distinct growth of these cones (c), so I stopped toluene flowing and scanned the cones (d) to obtain the topography of the sample. These cones are asymmetric with indented holes on the top. The depression at the rim existed the same as that in the PSc system. The tendency that aspect ratios and heights changed with time is shown in Figure 3.14.

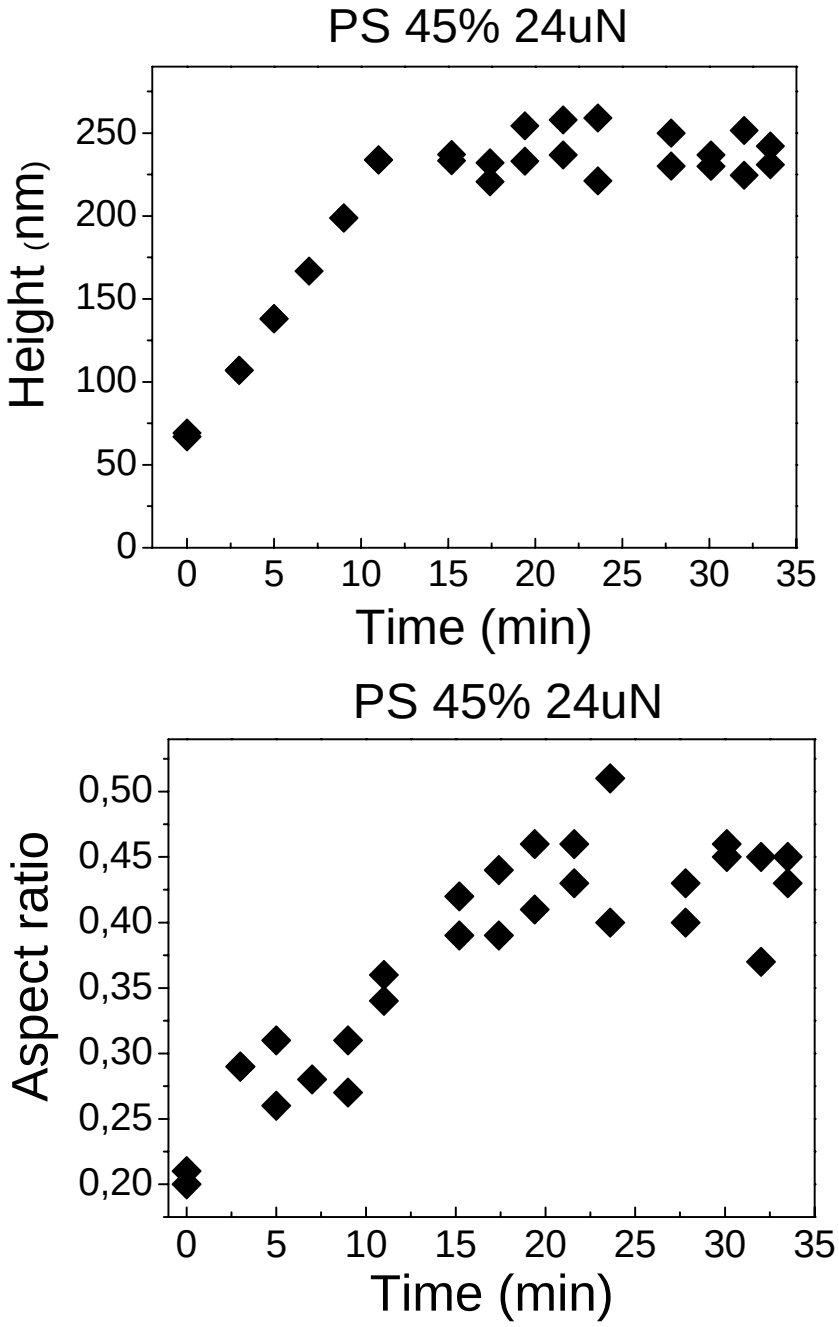

Figure 3.14 time dependence of height and aspect ratio, same experimental parameters as the figure 3.13

Figure 3.14 showed that in the first 10mins, the height was growing linearly. After reaching to 250nm, the height remained constant. The aspect ratio also showed a similar tendency: growing for 20mins, and after remaining mainly constant.

According to Equation (3), diffusion coefficient D equals to the square of penetration depth (d) divided by time t. The height h of the growing structures should be related to the depth of toluene penetrating to the substrate. The depth d is proportional to the square root of the product of D times t. If h is proportional to d, then it should also be proportional to the square root of t, Equation (4). In my experiment, instead, it grew linearly with time. The mechanism behind is not clear. There might be other processes more than swelling involved. So the height is not proportional to the depth of penetration.

$$D = \frac{d^2}{t} \qquad \text{Equation (3)}$$

$$h \propto d \propto \sqrt{Dt} \qquad \text{Equation (4)}$$

3.3.2 50% toluene concentration and 16μN force load indentation

When I used a higher toluene concentration and a lower initial indentation force load, I obtained a different result. In the Figure 3.15, the relative concentration of toluene is 50%. The indentation force load is 16μN, and the depth of the holes is 70nm. 18.9mins were needed to acquire every picture. The first image (a) was scanned after indentation under nitrogen. Toluene vapor was injected from the second one (b), and stopped at the last second (g). Arrows show the scan direction (the time axis). The last image was taken under nitrogen.

As toluene vapor was injected, the cones started growing. There was no obvious lateral expansion in Figure 3.14. In the following 100 minutes, these cones did not grow distinctly (c)~(g). Then I stopped toluene flowing and imaged the cones (h). The same as in Figure 3.13, the cones are asymmetric with indented holes on the top, and the depression at the rim. What should be noticed is that the scratch on the polystyrene surface swelled after 100 minutes (see green arrow). The rings in the blue circle are the artifact during image processing. The tendency of the aspect ratios and the heights changed with time is shown in Figure 3.16.

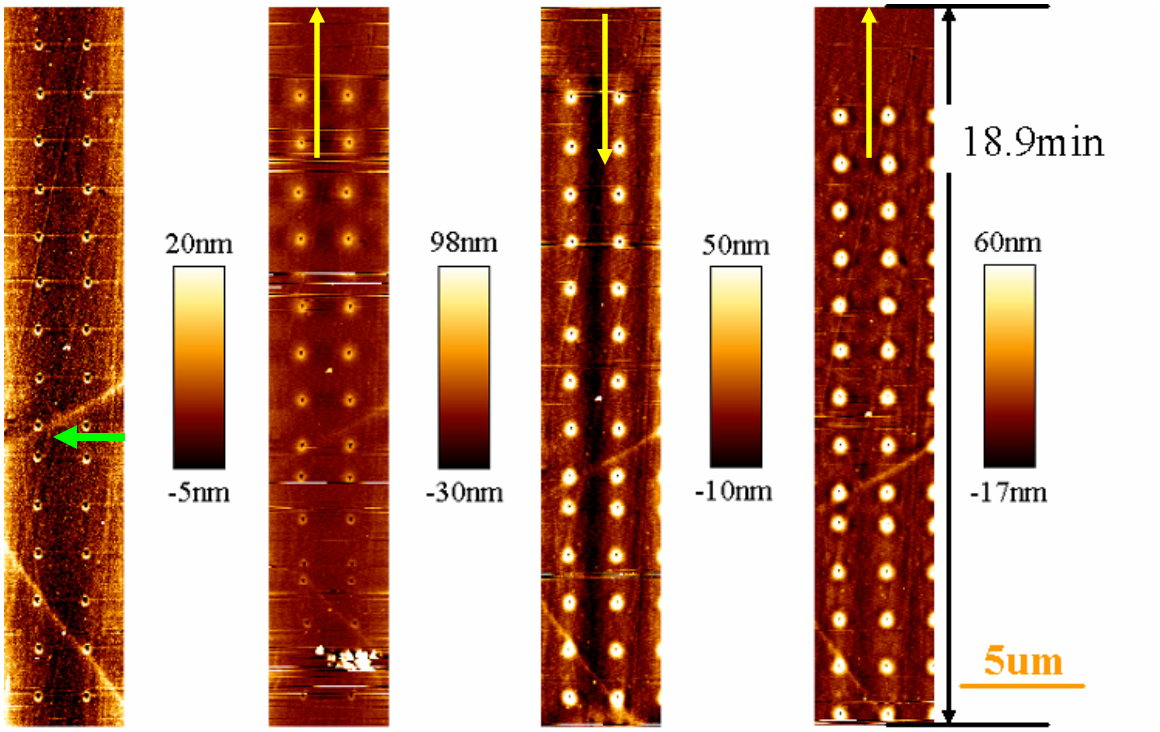

(a) (b) (c) (d)

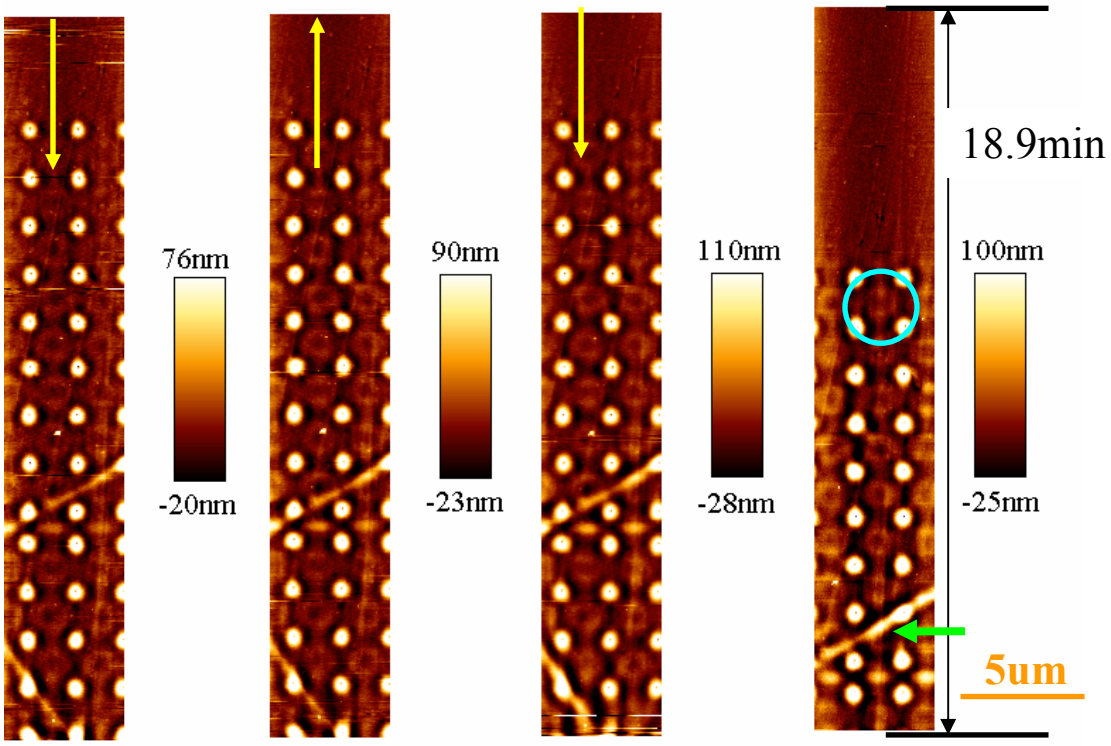

(e) (f) (g) (h)

Figure 3.15 In-situ systems with 50% concentration 16μN force load of initial force load.

In Figure 3.16, the time dependence of the height and the aspect ratio are different from those observed in Figure 3.14: the height did not stop growing for nearly two hours and only reached to 160nm. This is much lower than the height reached in the last experiment which is 240nm. Also the aspect ratio is only 0.3, lower than that in the 45%, 24μN system. The parameters are discussed in 3.3.3.

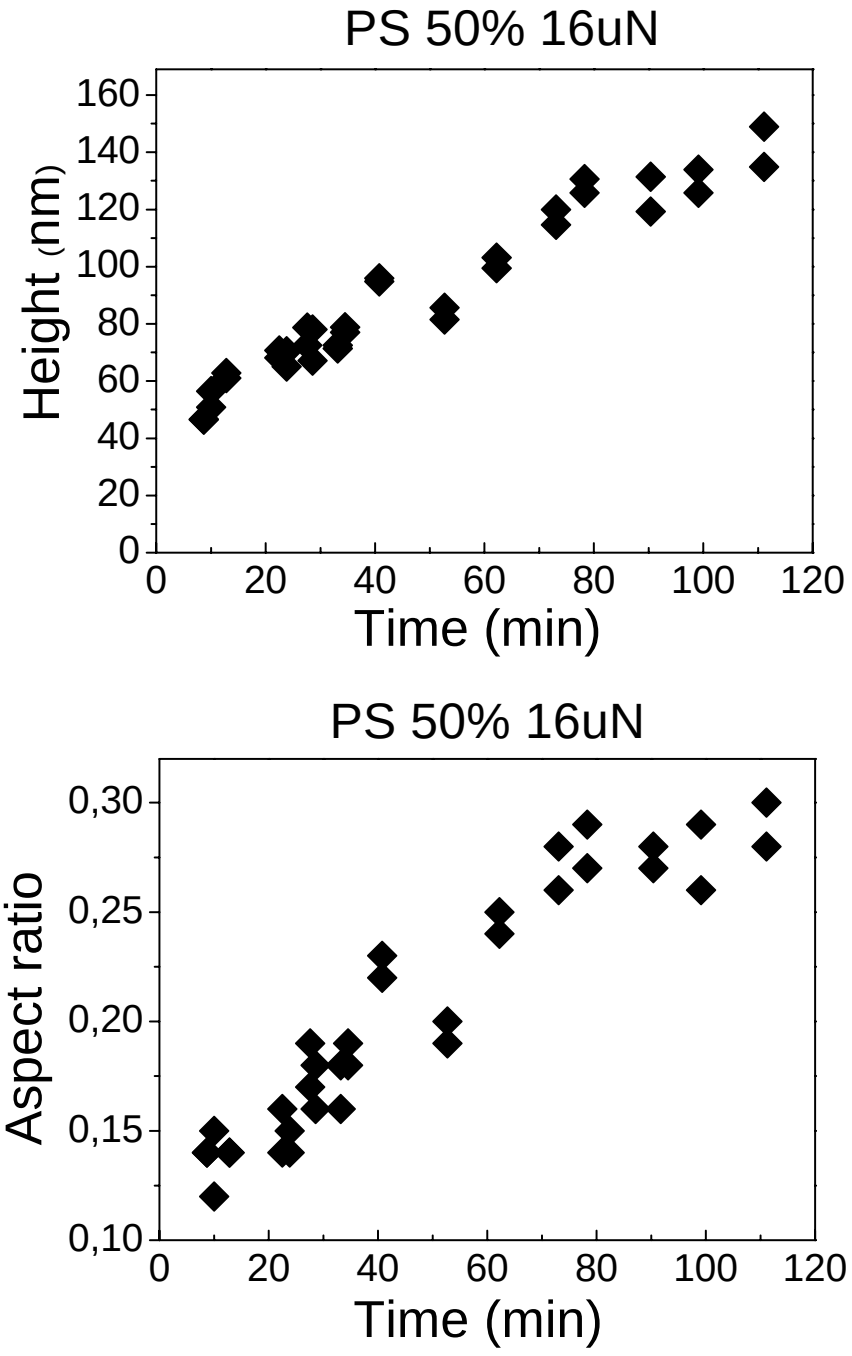

Figure 3.16 time dependence of height and aspect ratio

3.3.3 Summary of the in-situ system

To find the key parameters influencing the kinetics in the in-situ system, I compare initial indentation force load and toluene relative concentration in the systems: 45%, 24μN; 45%, 16μN; and 50%, 16μN.

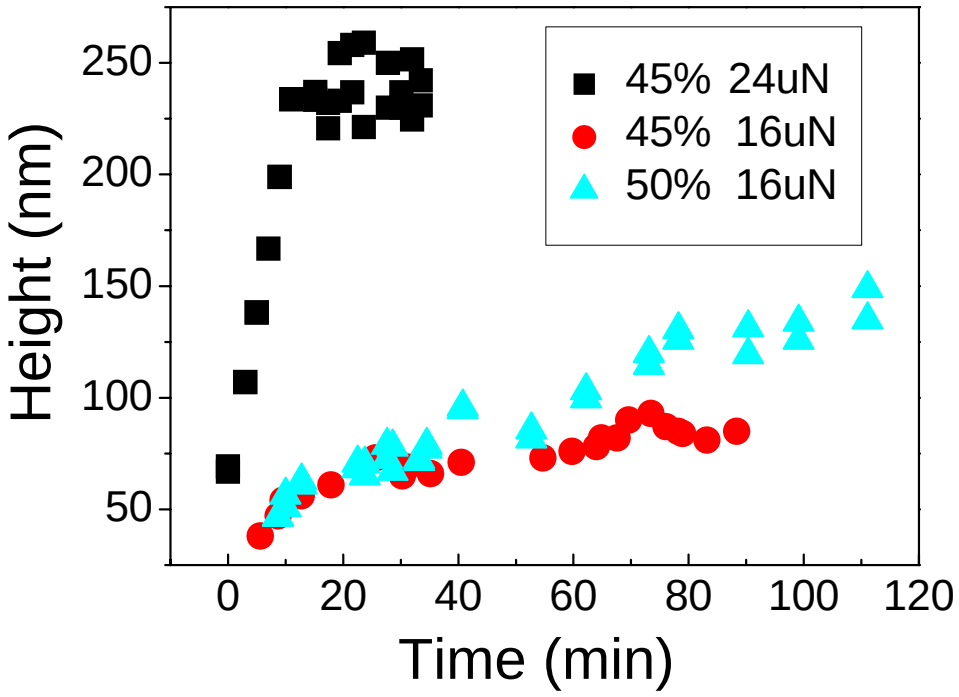

Figure 3.17 heights with different initial parameters.

Comparing the system of 45%, 24μN (black squares) with the system of 45%, 16μN (red dots), I found that under the same concentration, a large force load, which corresponds to a deeper hole, will lead to a faster growth. Compared the system of 45%, 16μN (red dots) and the system of 50%, 16μN (blue triangles), the conclusion is that with similar initial conditions, growth of the structures will be faster in higher concentrated toluene than that in lower concentrated. Compare the system of 45%, 24μN (black squares) with the system 50%, 16μN (blue triangles), we can also draw the conclusion that the size of the indented hole is more important than the concentration of toluene vapor during the swelling process for controlling the final height of the nanostructures. Still, one more issue must be pointed out: toluene leaking: it is almost impossible to have a closed system by using the O-ring, which is the only choice at the moment. So the concentration of toluene vapor in the closed cell might be different from the concentration set, also by more than 10% between different measurements.

3.4 Discussions about the mechanism of swelling process

After analyzing the systems in the ex-situ experiment and the in-situ experiment, I tried to figure out the mechanisms of swelling process.

In the PSc system, I compare profiles of a hole and two cones with different heights from sample 2. The result shows that the width (defined in 3.1) did not change much during swelling, and the growth of the cones is almost vertical, as shown in Figure 3.18.

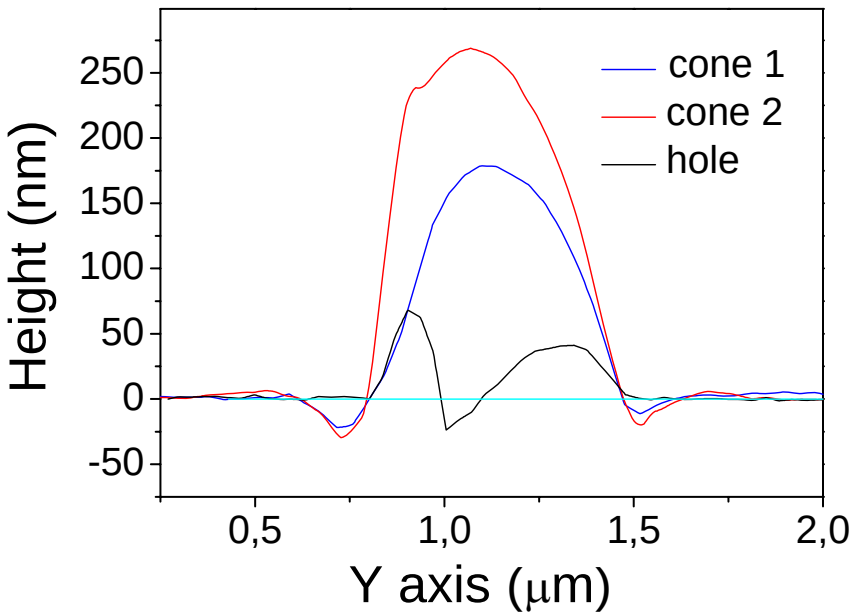

Figure 3.18 Profiles of a hole and two cones in PSc system

In the PSc-6nmAu system I also chose a hole and different high cones from a sample. From profiles shown in Figure 3.19 it is obvious that the growth of the cones is not only vertically, but they also expand laterally. The border wall is smaller than that in PSc system. The two cons have a similar figure.

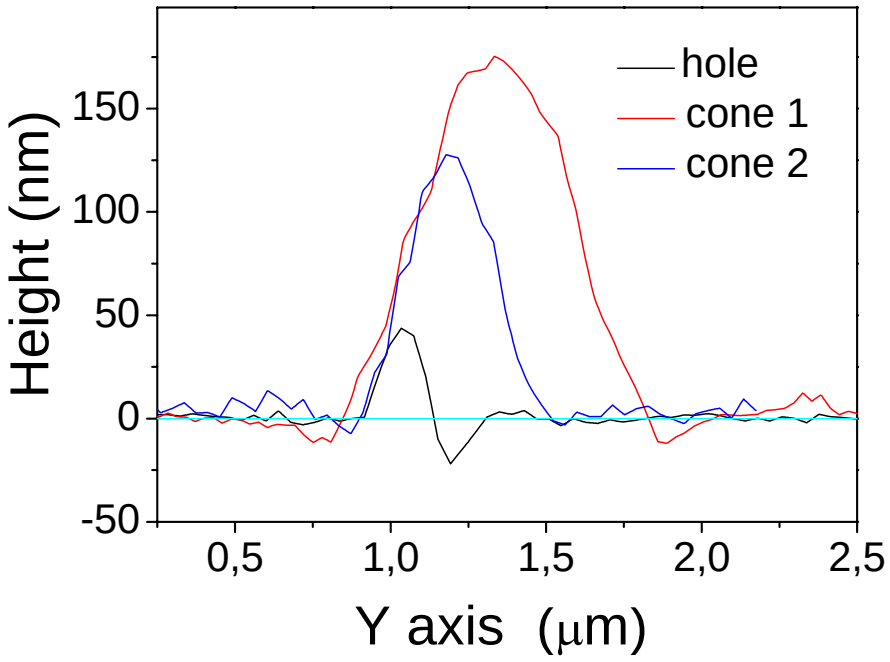

Figure 3.19 Comparison of hole and cones in PSc-Au system

The difference between two systems is only the 6nm thick gold layer sputtered on the surface of cross-linked polystyrene. In the PSc system the superficial cross-linked layer can protect the whole surface from swelling, but can not prevent toluene to penetrate through it. In the PSc-Au system the 6nm thick gold layer can not protect the surface from swelling and being penetrated by toluene vapor, but it can slow down the velocity of toluene vapor diffusing through it.

The averaged values and standard deviations of the height, width, and aspect ratio for the two systems, PSc (swelling time: 30s) and PSc-6nmAu (swelling time: 60s), are summarized in Table 5. At least 10 structures were calculated. Distribution is calculated by standard deviation divided by the average.

Table 5 height, width, and aspect ratio distribution of PSc system and PSc-Au

PSc 30s	**h(height)**	**w(width)**	**aspect ratio**
average	224nm	0,35μm	0,64
standard deviation	31nm	0,02μm	0,07
distribution	14%	5%	11%

PSc-Au 60s	h(height)/nm	w(width)/μm	aspect ratio
average/nm	137nm	0,35μm	0,39
standard deviation/nm	28nm	0,07μm	0,04
distribution	20%	19%	9%

From the distribution, the tendency is clear: in the PSc system, the cones maintain the same width, while in the PSc-Au system the cones maintain the same aspect ratio. This is probably due to the fact that in the PSc system swollen polystyrene is squeezed out of the surface faster because of the high velocity of toluene penetration. So a large amount of toluene vapor penetrated the whole surface in a short time, and the swollen polystyrene was squeezed out through the holes indented by AFM tip. In this way, the original width of the hole carved in the cross-linked polystyrene layer does not change during the formation of the cones. In the PSc-6nmAu system polystyrene swelled slowly due to the presence of the gold layer. Swollen polystyrene flowed out of the holes and formed a certain angle on the surface. So the aspect ratio of PSc-Au would like to keep constant, and the cones have a similar figure.

If the thickness of the gold layer is larger than 10nm, the velocity of toluene penetration is so slow, that there is only a little polystyrene swelled in several minutes (Figure 3.20). The depth of the holes reduced, which means the polystyrene swelled. The height of the "cone" remained almost the same as the height of the border wall, which implies that the toluene vapor may be impeded to go through the 10nm Au layer.

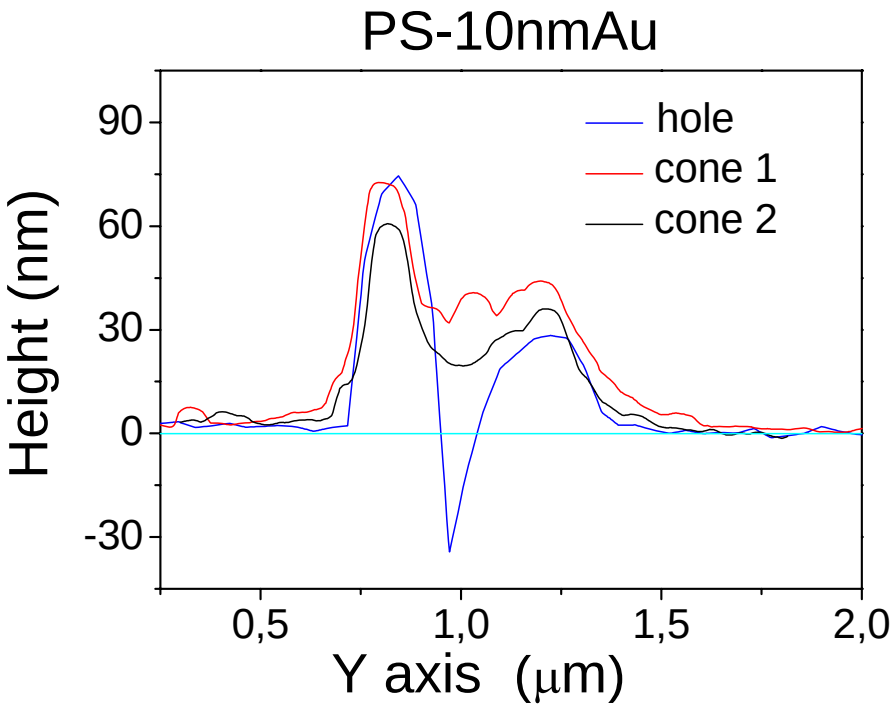

Figure 3.20 Comparison of hole and cones in the PS-Au system

In the in-situ system, polystyrene was treated the same way as in the PSc system (60W, 4min), so the profiles of cones should be the same. Figure 3.21 shows the growth of the cone with time in the in-situ system: the cones grew vertically and laterally. While in the PSc system, the cones grew only vertically. The difference between two systems is the reduced concentration of the toluene vapor. This will not slow down the penetration velocity of toluene, but the amount of toluene vapor. The superficial cross-linked polystyrene layer was swelled after exposing to the solvent for a long time, which is not the case in the ex-situ system. So the profiles are not exactly the same: the width also grew with time in the in-situ system.

$$D(T) = D_0 \times e^{-\frac{E}{RT}} \qquad \text{Equation (5)}$$

D(T): diffusion coefficient
D_0: maximum diffusion coefficient
E_A: activation energy for diffusion
T: absolute temperature
R: gas constant

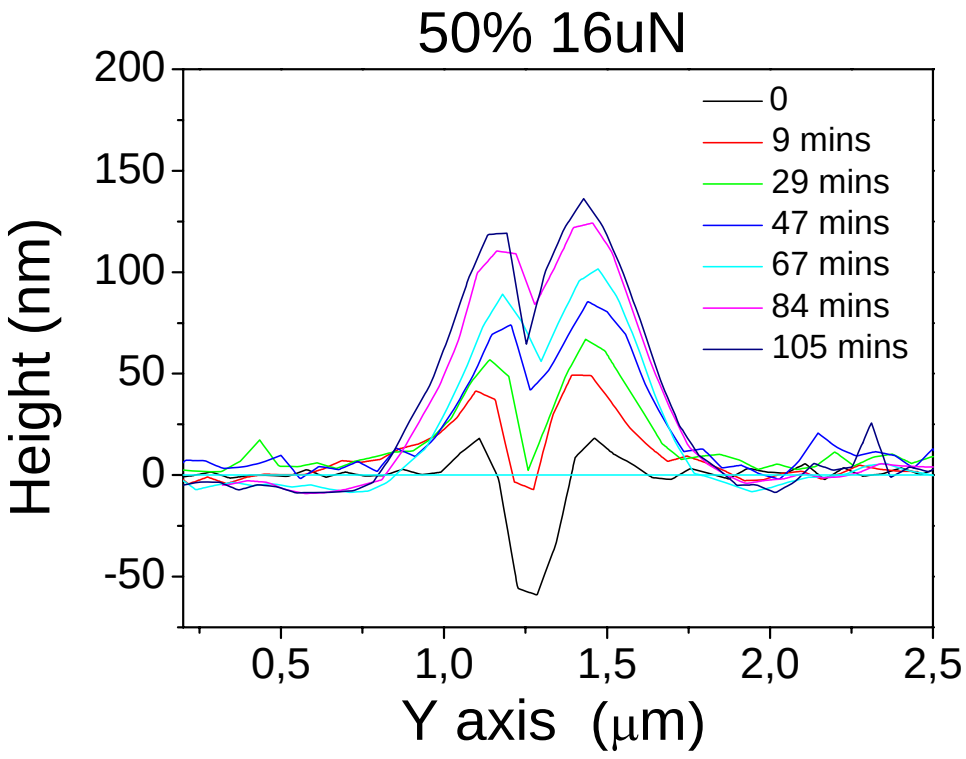

Figure 3.21 Growth of a cone in in-situ system

The mechanism behind this process is complex, and it is too early to draw a conclusion. From my experiments, it looks like the mechanisms are several, but depending on the properties, resistance of surface to toluene penetration, deformation of the surface, surface energy, swelling time, etc. If a large amount of the toluene vapor penetrates non-cross-linked polystyrene in a short time, then the swollen polystyrene is squeezed out via the hole. It looks like flowing mechanism in PSc and PSc-Au systems. When the velocity of toluene vapor penetration is not large enough, swelling mechanism may dominate the process, such as in the PS-10nmAu system. Both mechanisms could work on one system, if the surface swells after exposure to the solvent vapor.

3.5 Thickness of cross-linked polystyrene layer

It is difficult to measure the thickness of cross-linked polystyrene layer by optical methods. So I scratched lines on the polystyrene surface by static plowing to find out the depth of the cross-linked layer.

The sample was treated as before: exposed to plasma for 4mins with 60W. The tip was a tapping mode tip with spring constant of 42N/m. It was operated in contact mode and scanned along the designed lines with different force loads, from 3μN to 10μN. In Figure 3.22 (a), there were five lines in a square. The square was plowed by 3μN force load, and five lines were plowed by the force load of 3μN, 5μN, 7μN, 9μN and 10μN from left to right respectively. Figure 3.22 (b) shows structures formed after exposed to solvent vapor for 60s.

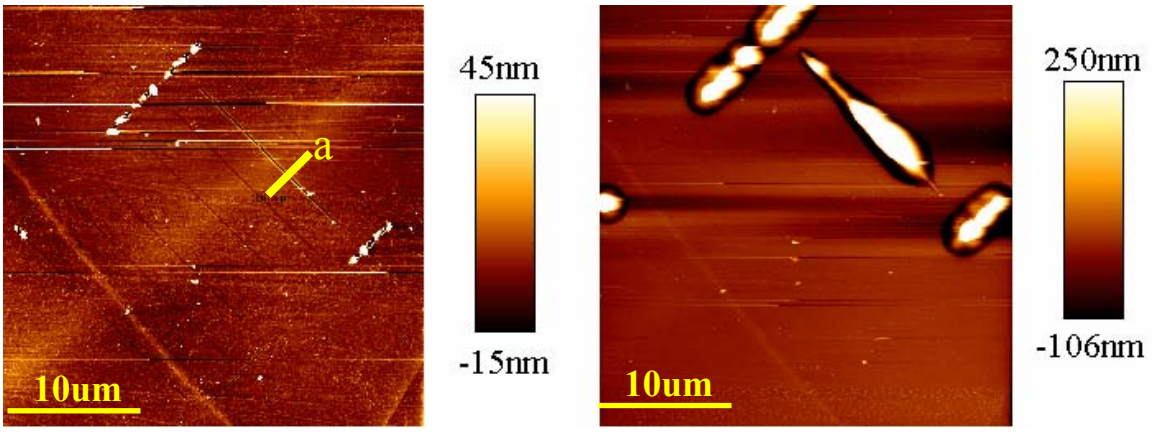

(a) after static plowing (b) after swelling

Figure 3.22 Images of lines done by static plowing before and after swelling

The structure only can form where the cross-linked polystyrene layer is pierced. So it is easy to obtain the information about the thickness of the cross-linked layer from the profile (Figure 3.23). The thickness of the layer is between 13~20nm.

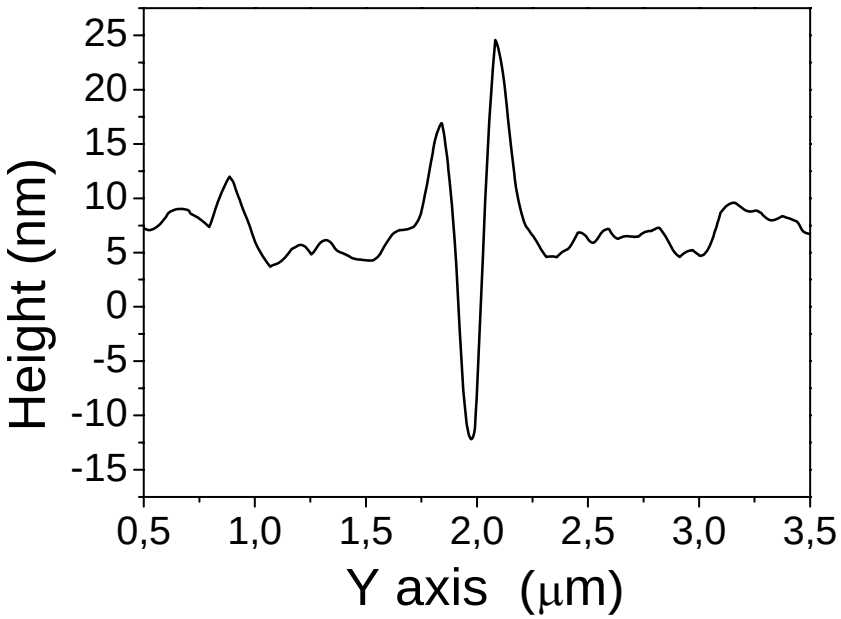

Figure 3.23 Z profile of plowing line a

4. Summary

Solvent-assisted nanolithography can generate relief structures on polystyrene surfaces. To find out the possibilities to control the aspect ratio, the height and the width, and understand the mechanism behind this process, I tried both ex-situ experiments and in-situ experiments.

In the ex-situ experiments, I tried to modify the surface properties of polystyrene by sputtering gold layer and attaching thiols. Different aspect ratios were obtained from PSc system, Ps-Au-CH_3 system, PS-Au system, PSc-Au system, PSc-Ti-Au system and PSc-Ti-Au-CH_3 system.

a) The plasma treated polystyrene, the PSc system, provides the highest aspect ratio which is between 0.5 and 0.6

b) The structures formed from PSc-6nmAu system have the aspect ratio between 0.3~0.4.

c) The systems with thicker gold layers and titanium layers, which are PS-10nmAu, PS-16nmAu, PSc-2nmTi-6nmAu, and PSc-2nmTi-Au-CH_3, formed the structures with aspect ratio between 0.1~0.2.

The plasma treated polystyrene, PSc system, provides the highest aspect ratio due to the highest penetration velocity of toluene vapor. The system with thin gold layers, PSc-6nmAu, provides lower aspect ratio, because the existence of the gold layer slows down the penetration of toluene vapor. The lowest aspect ratios are provided by the systems with thicker gold layer and titanium layer, such as PS-10nmAu, PS-16nmAu, PSc-2nmTi-6nmAu, and PSc-2nmTi-6nmAu-CH_3 systems. In these systems, toluene can not penetrate the superficial layer, but the only breakthrough holes. So only few material around the holes swelled.

To study kinetics behind this process, I used the in-situ experiments with gas mass flow control setup to monitor the samples during swelling. In the kinetics study, several conclusions are drawn:

a) In the condition of the same initial parameters, the growth of the structures will be faster in higher toluene concentration than in lower concentration.

b) If the concentrations of toluene vapor are the same, a larger indentation force load leads to a faster growth.

c) Compared to concentration of toluene vapor, the initial hole depth is more important.

5. Conclusion

The surface properties make difference in swelling process. Instead of the different surface energies as we expected, the main reason that surface properties influence the whole process is due to the different penetration velocities of toluene vapor. Surface modification experiments are not enough to reveal the mechanism of swelling process, but show the importance of kinetics study.

The kinetics is studied by the in-situ experiments, in which I monitored the samples during swelling. I find that the initial force load is the key parameter to control the final height in the swelling. There are two challenges in the in-situ experiments: first is to control concentration of toluene vapor in AFM cell precisely; second is to reduce exposure time of cross-linked polystyrene due to the surface swelling problem. The results of the ex-situ experiment and in-situ experiment show the possibility that the mechanism behind the process is not unique, but depends on the situations.

In the future experiments, changing surface energy without effecting toluene penetration is the direct way to study mechanism, although it will be difficult. Plasma treatment by different gas can be used to modify surface energy of cross-linked polystyrene. Another way is to study the kinetics of surface modified polystyrene. This can be done by in-situ system. Instead of commercial polystyrene plates, we also can use homemade pure polystyrene by which different properties, like molar mass or PDI, can be easily controlled.

If we can figure out the mechanism and kinetics behind, then it is possible to control the process to form structures with a high aspect ratio and apply it into more applications.

6. Acknowledgements

First I sincerely acknowledge **Dr. Ramon Pericet-Cámara**, and **Dr. Elmar Bonaccurso**, for good supervision. I also would like to thank **Dr. Brunero Cappella** for the invaluable discussion, and suggestions. Thanks are given to **Uwe Rietzler** and **Dr. Svetlana Guriyanova** for introducing me to AFM and Force curve measurements, **Maren Müller** for the SEM imaging of the cantilevers, and **Dr. Masaya Toda** for generous help with the mass flow control setup.

I also give my appreciation to **Prof. Dr. Hans-Jürgen Butt**, for giving me the precious chance to work in his department in Max-Planck Institute for Polymer Research for my master thesis work, and **Prof. Dr. Bernward Engelen** for offering me the opportunity to join the International Graduate Studies in University Siegen.

Finally I thank all the members in AK-Butt of Max-Planck Institute for Polymer Research for the nice working atmosphere, generous help and fruitful suggestions.

7. Reference

[1]X.N. Xie, H.J. ChμNg, C.H. Sow, A.T.S. Wee, *Nanoscale materials patterning and engineering by atomic force microscopy nanolithography*, Materials Science and Engineering R 54 (**2006**) 1–48

[2] H. Klauk, D.J. GμNdlach, M. Bonse, C.C. Kuo, T.N. Jackson, *A reduced complexity process for organic thin film transistors*, Appl. Phys. Lett. 76 (**2000**) 1692.

[3] J.G. Goodberlet, *Patterning 100 nm features using deep-ultraviolet contact photolithography*, Appl. Phys. Lett. 76 (**2000**) 667.

[4] J. Fujita, Y. Ohnishi, Y. Ochiai, S. Matsui, *Photon-assisted resonant tμNneling through variably spaced superlattice energy filters*, Appl. Phys. Lett. 68 (**1996**) 1297.

[5] A.P.G. Robinson, R.E. Palmer, T. Tada, T. Kanayama, J.A. Preece, *A Fullerene derivative as an electron beam resist for nanolithography*, Appl. Phys. Lett. 72 (**1998**) 1302.

[6] S. Rennon, L. Bach, J.P. Reithmaier, A. Forchel, J.L. Gentner, L. Goldstein, *High-frequency properties of 1.55 μm laterally complex coupled distributed feedback lasers fabricated by focused-ion-beam lithography*, Appl. Phys. Lett. 77 (**2000**) 325.

[7] L. Bach, I.P. Reithmaier, A. Forchel, J.L. Gentner, L. Goldstein, *Multiwavelength laterally complex coupled distributed feedback laser arrays with monolithically integrated combiner fabricated by focused-ion-beam lithography*, Appl. Phys. Lett. 79 (**2001**) 2324.

[8] T. H. Fang, C. I. Weng and J. G. Chang, *Machining characterization of the nano-lithography process using atomic force microscopy*, (**2000)** Nanotechnology 11 181–7

[9] R. Magno and B. R. Bennett, *Nanostructure patterns written in III–V semiconductors by an atomic force microscope*, Appl. Phys. Lett. 70 **(1997)**1855–7

[10] Bouchiat V and Esteve D, *Lift-off lithography using an atomic force microscope*, Appl. Phys. Lett. 69 (**1996**)3098–100

[11] Sugihara H, Takahara A and Kajiyama T, *Mechanical nanofabrication of lignoceric acid monolayer with atomic force microscopy*, J. Vac. Sci.Technol. B 19(**2001**) 593–5

[12] Loi S, Wiesler U M, Butt H-J and Müllen K, *Self-Assembly of Alkyl-Substituted Polyphenylene Dendrimers on Graphite*, Macromolecules 34(**2001**) 3661–71

[13] Brunero Cappella and Elmar Bonaccurso, *Solvent-assisted nanolithography on polystyrene surfaces using the atomic force microscope*, Nanotechnology 18 (**2007**) 155307 (6pp)

[14] Binnig, G., Quate, C.F., and Gerber, C., *Atomic Force Microscope*, Phys. Rev. Lett., 56,(**1986**) 930-933.

[15] H.-J. Butt, B. Cappella, M. Kappl, Force *measurements with the atomic force microscope: Technique, interpretation and applications*, Surface Science Reports 59 (**2005**) 1–152

[16] B. Cappella, handout from lecture

[17] E. Bonaccurso PhD thesis, *Investigation of electrokinetic forces on single particles*

[18] B. Cappella, H. Sturm, S.M. Weidner, Breaking *polymer chains by dynamic plowing lithography*, Polymer 43 (**2002**) 4461.

[19] M. Heyde, K. Rademann, B. Cappella, M. Geuss, H. Sturm, T. Spangenberg, H. Niehus, *Dynamic plowing nanolithography on polymethylmethacrylate using an atomic force microscope*, Rev. Sci. Instrμm. 72 (**2001**) 136.

[20] B. Cappella and H. Sturm, *Comparison between dynamic plowing lithography and nanoindentation methods*, J. Appl. Phys. Vol 91, NUMBER 1

[21] M, Strobel, C.Lyons, K. Mittal; *Plamsa surface modification of polymers: relevance to adhesion*; VSP publications; (**1994**)

[22] www.wikipeida.org

[23] Jeremy M. Grace a; Louis J. Gerenser b, *Plasma Treatment of Polymers*, Journal of Dispersion Science and Technology, Vol. 24, Nos. 3 & 4, pp. 305–341, (**2003**)

[24] N. D. Tran, N. K. Dutta, and N. R. Choudhury, *Plasma-polymerized perfluoro(methylcyclohexane) coating on ethylene propylene diene elastomer surface: Effect of plasma processing condition on the deposition kinetics, morphology and surface energy of the film*, Thin Solid Films 491, 123 (**2005**).

[25] C. Chan, *Polymer surface modification and characterization*; Hanser: München, (**1994**), Chap. 1 P19

[26] H. K. Yasuda, Y.S. Yeh, and S. Fusselman, *A growth mechanism for the vacuum deposition of polymeric materials*, Pure Appl. Chem.62, (**1990**),1689

[27] http://www.espi-metals.com/

[28] A. W. Adamson; A. P.Gast, *Physical Chemistry of Surfaces*, 6th ed.; Wiley-Interscience: New York, (**1997**).

[29] J. Christopher Love, Lara A. Estroff, Jennah K. Kriebel, Ralph G. Nuzzo, and George M. Whitesides, *Self-Assembled Monolayers of Thiolates on Metals as a Form of Nanotechnology*, Chem. Rev. 105, (**2005**),1103-1169

[30] L. H. Dubois; R. G.Nuzzo, *Synthesis, Structure, and Properties of Model Organic Surfaces*, Annu. Rev. Phys. Chem. 43, (**1992**),437.

[31] L. H. Dubois; B. R. Zegarski; R. G. Nuzzo, *Molecular ordering of organosulfur compoμNds on Au(111) and Au(100): Adsorption from solution and in ultrahigh vacuum*, J. Chem. Phys. 98, (**1993**)678.

[32] F.Schreiber, *Structure and growth of self-assembling monolayers*, Prog. Surf. Sci.65,(**2000**)151.

[33] G. E. Poirier, *Characterization of Organosulfur Molecular Monolayers on Au(111) using Scanning Tunneling Microscopy*, Chem. Rev. 97, (**1997**)1117.

[34] A. Ulmann, *Self-Assembled Monolayer of thiols*; Academic Press: New York. (**1998**)

[35] G. Li, PhD thesis, *Structuring of polymer surface by evaporation of sessile microdrops*

[36] J. Wang, master thesis, *Analysis of Dialkyldisulfide Monolayers on Gold by Atomic Force Microscopy*

[37] A. Larsson,; H. De´randy, , *Stability of Polycarbonate and Polystyrene Surfaces after Hydrophilization with High Intensity Oxygen RF Plasma*, J. Colloid Interface Sci. 246, (**2002**)214.

[38] E. Bonaccurso, B. Cappella and K. Graf, *Local Mechanical Properties of Plasma Treated Polystyrene Surfaces*, J. Phys. Chem. B110 (**2006**) 17918–24

[39] E. Bonaccurso and K. Graf, *Nanostructuring Effect of Plasma and Solvent Treatment on Polystyrene*, Langmuir 20 (**2004**)11183–90

[40] Bonaccurso E, Butt H-J and Graf K, *HerstellµNg von Arrays aus Mikroreaktionst¨opfen Mittels L¨osungsmitteld¨ampfen German Patent Application* 102 (**2002**)53 077.7

[41] E. Bonaccurso, H.-J. Butt and K. Graf, *Microarrays by structured substrate swelling*, Eur. Polym. J.40 (**2004**) 975–80

[42] P. West and N. Starostina, AFM image artifacts

8. Appendix

Initial parameter

Depth is defined in 3.1. W1 and w2 are defined in Figure 1to study.

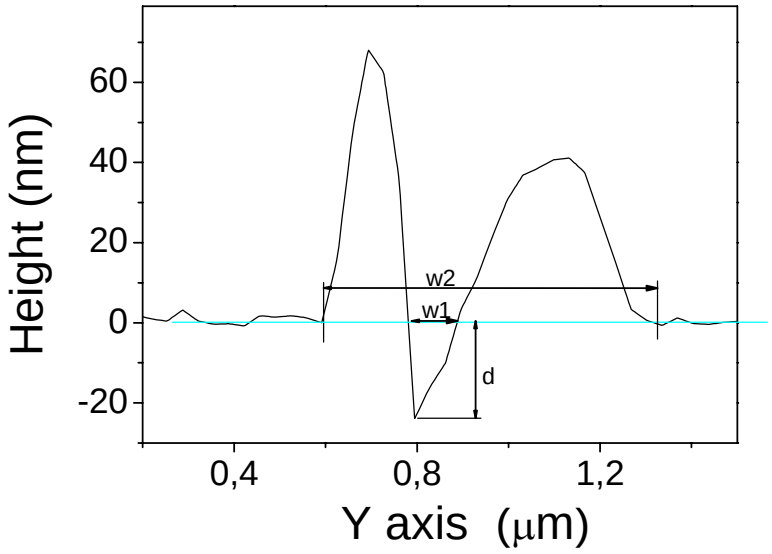

Figure 1. Definitions about holes

Table 1 and Table 2 are the initial conditions and swelling parameters of different samples of ex-situ system. Every date is the average of 10 to 30 cones or holes from one sample.

As we can see a larger force load always leads to a deeper holes and wider border wall. There is no clear dependence of aspect ratio on the exposing time.

Table 1. Initial conditions of different systems

system	thickness	Indentation				swelling			
		force load	depth/nm	width1/nm	width2/nm	time/s	height/nm	width/nm	aspect ratio
PSc		24μN	10±3	57±9	719±22	60	172±4	341±4	0,50±0,01
		20μN	27±3	104±12	727±29	30	224±31	352±17	0,64±0,07
PS-Au-CH3	Au:20nm	24μN	62±12	305±33	538±48	120	130±29	417±42	0,31±0,05
						120+120	142±23	433±43	0,,33±0,04
		16μN	40±6	187±13	416±43	120	remain the same		
						120+120			
PSc-Au	Au:6nm	24μN	17±6	145±26	585±48	60	137±28	352±65	0,39±0,04
						60+60	126±21	377±53	0,33±0,02
PSc-Ti-Au	Au:6nm Ti:2nm	20μN	18±4	144±23	455±50	60+60	63±6	366±16	0,17±0,02
PSc-Ti-Au-CH3	Au:6nm Ti:2nm	24μN	24±5	171±26	592±54	60	no data available		
						120s	42±7	286±37	0,14±0,02